Clostridioides difficile-mucus interactions encompass shifts in gene expression, metabolism, and biofilm formation.

Kathleen L. Furtado[a], Lucas Plott[b], Matthew Markovetz[b], Deborah Powers[c], Hao Wang[d], David B. Hill[b,e,f], Jason Papin[c,g,h], Nancy L. Allbritton[d], and Rita Tamayo[a]#

[a]Department of Microbiology and Immunology, University of North Carolina at Chapel Hill School of Medicine, Chapel Hill, NC, USA

[b]Marsico Lung Institute, University of North Carolina at Chapel Hill School of Medicine, Chapel Hill, NC, USA

[c]Department of Biochemistry and Molecular Genetics, University of Virginia, Charlottesville, VA, USA

[d]Department of Bioengineering, University of Washington, Seattle, WA, USA.

[e]Joint Department of Biomedical Engineering, University of North Carolina at Chapel Hill, Chapel Hill, NC, USA

[f]Department of Physics and Astronomy, College of Arts and Sciences, University of North Carolina at Chapel Hill, Chapel Hill, NC, USA

[g]Department of Biomedical Engineering, University of Virginia, Charlottesville, VA, USA

[h]Department of Medicine, Division of Infectious Diseases and International Health, University of Virginia, Charlottesville, VA, USA

#Corresponding author

125 Mason Farm Rd, CB #7290

Chapel Hill, NC 27599-7290

+1 (919) 843-2864

rita_tamayo@med.unc.edu

ABSTRACT

In a healthy colon, the stratified mucus layer serves as a crucial innate immune barrier to protect the epithelium from microbes. Mucins are complex glycoproteins that serve as a nutrient source for resident microflora and can be exploited by pathogens. We aimed to understand how the intestinal pathogen, *Clostridioides diffiicile*, independently uses or manipulates mucus to its benefit, without contributions from members of the microbiota. Using a 2-D primary human intestinal epithelial cell model to generate physiologic mucus, we assessed *C. difficile*-mucus interactions through growth assays, RNA-Seq, biophysical characterization of mucus, and contextualized metabolic modeling. We found that host-derived mucus promotes *C. difficile* growth both *in vitro* and in an infection model. RNA-Seq revealed significant upregulation of genes related to central metabolism in response to mucus, including genes involved in sugar uptake, the Wood-Ljungdahl pathway, and the glycine cleavage system. In addition, we identified differential expression of genes related to sensing and transcriptional control. Analysis of mutants with deletions in highly upregulated genes reflected the complexity of *C. difficile*-mucus interactions, with potential interplay between sensing and growth. Mucus also stimulated biofilm formation *in vitro*, which may in turn alter viscoelastic properties of mucus. Context-specific metabolic modeling confirmed differential metabolism and predicted importance of enzymes related to serine and glycine catabolism with mucus. Subsequent growth experiments supported these findings, indicating mucus is an important source of serine. Our results better define responses of *C. difficile* to human gastrointestinal mucus and highlight a flexibility in metabolism that may influence pathogenesis.

IMPORTANCE

Clostridioides difficile results in upwards of 250,000 infections and 12,000 deaths annually in the United States. Community-acquired infections continue to rise and recurrent disease is common, emphasizing a vital need to understand *C. difficile* pathogenesis. *C. difficile*

53 undoubtedly interacts with colonic mucus, but the extent to which the pathogen can
54 independently respond to and take advantage of this niche has not been explored extensively.
55 Moreover, the metabolic complexity of *C. difficile* remains poorly understood, but likely impacts
56 its capacity to grow and persist in the host. Here, we demonstrate that *C. difficile* uses native
57 colonic mucus for growth, indicating *C. difficile* possesses mechanisms to exploit the mucosal
58 niche. Furthermore, mucus induces metabolic shifts and biofilm formation in *C. difficile*, which
59 has potential ramifications for intestinal colonization. Overall, our work is crucial to better
60 understand dynamics of *C. difficile*-mucus interactions in the context of the human gut.
61

62 **INTRODUCTION**

63 As the leading cause of hospital-acquired diarrhea, *Clostridioides difficile* remains an
64 urgent public health threat[1]. Although typically classified as a nosocomial pathogen, community-
65 acquired cases of *C. difficile* infection (CDI) now comprise almost half the total number of
66 cases[1]. As recurrent CDI affects nearly 50% of first-time patients[2], a better mechanistic
67 understanding of *C. difficile* pathogenesis is crucial to breaking this debilitating cycle. As an
68 obligate anaerobe transmitted via spores, *C. difficile* germinates within the small intestine and
69 establishes infection in the colon. *C. difficile* possesses mechanisms to directly adhere to the
70 epithelium during colonization, including surface layer proteins[3,4], flagella[5], type IV pili[6], and
71 binary toxin in certain epidemic isolates[7–9]. Before accessing the epithelium, *C. difficile* must
72 interact with colonic mucus, a key feature of innate host immunity.

73 The colonic mucus barrier is stratified, consisting of a diffuse luminal layer of secreted
74 mucins inhabited by commensal microbes and a relatively sterile layer of membrane-bound
75 mucins. The predominant secreted mucin in the colon is MUC2. Among membrane-bound
76 mucins, MUC1 is particularly important in protection from bacterial invasion[10]. Past work
77 suggests *C difficile* associates with the mucus barrier at multiple levels. Studies using animal
78 colonization models indicate *C. difficile* inhabits the outer mucus layer[11], while others showed

79 co-localization of *C. difficile* and mucus in CDI patient stool samples, which are particularly rich
80 in MUC1[12]. Subsequent work demonstrated direct adherence of *C. difficile* to purified MUC2[13].
81 This evidence indicates mucus serves as an anchoring point for *C. difficile* during colonization.
82 Mucins are heavily glycosylated, with O-glycans decorating both MUC1 and MUC2 and
83 N-glycans present on MUC1[10,14,15]. Glycans contribute to 80% of the mass of MUC2, and thus
84 make up a significant proportion of mucin[16]. These glycans can be degraded by several
85 bacterial species, providing a rich source of carbohydrates to the microbiota. Monosaccharides
86 available from colonic mucins include fucose, mannose, galactose, N-acetylglucosamine
87 (GlcNAc), N-acetylgalactosamine, and N-acetylneuraminic acid[14,15]. Following glycan cleavage,
88 the peptide backbone also provides nutrients to the microbiota[14]. These backbones are rich in
89 serine, threonine, and proline[14,17]. In humans, nearly 45% of the amino acid composition of
90 MUC1 and over 55% of MUC2 consists of serine, threonine, and proline based on canonical
91 sequences in UniProt (P15941 and Q02817, respectively); others have predicted greater
92 proportions of these amino acids[18]. Overall, interactions between commensal microbiota and
93 mucus are often symbiotic, resulting in a thicker, more protective mucus layer for the host and
94 increased nutrient availability for the microbiota[14,19]. To maintain healthy conditions, mucin
95 degradation by bacteria and regeneration by the host must be carefully balanced.
96 Pathogens can alter and exploit mucus during infection[10]. Previous work showed that
97 oligosaccharide composition within mucus is altered during CDI, and that *C. difficile* reduces
98 expression of human *MUC2* while preferentially interacting with MUC1[12]. *C. difficile* also benefits
99 from the cleavage of mucins by specific members of the microbiota[20], however, the extent to
100 which mucus is altered or metabolized specifically by *C. difficile* remains unclear. The
101 carbohydrate active enzymes (CAZy) database indicates *C. difficile* R20291 possesses
102 enzymes from 31 families[21], at least one of which, glycosyl hydrolase family 38, contains
103 enzymes likely involved in mucin degradation[20]. To our knowledge, no study has assessed the

104 mucolytic capacity of any enzymes listed in the CAZy database for *C. difficile*. Nonetheless,
105 evidence to date indicates that alterations to mucus promote *C. difficile* colonization.
106 There are substantial challenges in obtaining mucus that accurately recapitulates native
107 human mucus in its composition and viscoelasticity[22], properties likely vital to *C. difficile*-mucus
108 interactions. Human mucus varies from that of animal models, and the processing of
109 commercial mucins removes important components from native mucus and disrupts its
110 structure[23]. Furthermore, immortalized colonic cell lines often do not secrete the same
111 proportions of mucin types as those in a healthy colon, if mucins are secreted at all[23–25].
112 Recently, a human primary intestinal epithelial cell (IEC) co-culture system was validated for use
113 with *C. difficile*[26]. These IECs can secrete a thick mucus barrier[27], which can be harvested or
114 directly inoculated to assess *C. difficile*-mucus interactions. Importantly, the biophysical
115 properties and composition of IEC-derived mucus are similar to mucus derived from *ex vivo*
116 human tissues[28].
117 The goal of this study was to assess specific interactions between *C. difficile* and human
118 colonic mucus to better understand the extent to which *C. difficile* can independently use or
119 manipulate mucus to its benefit. Using the physiologically relevant, primary IEC-derived mucus
120 described above, we measured the contribution of mucus to *C. difficile* growth. We then used
121 transcriptomics to explore the response of *C. difficile* to mucus and used these data in metabolic
122 modeling to predict how mucus shapes *C. difficile* metabolism. We additionally assessed the
123 capacity of *C. difficile* to alter biophysical and biochemical properties of mucus. Our work
124 provides a multi-faceted understanding of *C. difficile*-mucus interactions, which may influence
125 colonization or disease progression.
126
127 **RESULTS**
128 **Mucus derived from primary human IECs promotes *C. difficile* growth**

129 To test whether colonic mucus derived from primary human IECs supports or promotes
130 *C. difficile* growth, we examined growth *in vitro* in *C. difficile* minimal medium (CDMM)[29]
131 containing 1% glucose with and without 50 μg/mL mucus. We also tested conditions without
132 glucose, wherein mucus was the only source of sugars. All media tested supported *C. difficile*
133 growth due to the presence of casamino acids. In the presence of mucus, *C. difficile* exited lag
134 phase earlier and reached higher maximum OD_{600} than without mucus, both with and without
135 glucose (Fig 1A).
136 In CDMM with glucose, the addition of mucus resulted in faster growth rates (k) during
137 exponential phase (k = 0.176±0.013 OD_{600}/hour) compared to the no-mucus condition (k =
138 0.140±0.004 OD_{600}/hour) (Fig 1B). At 24h, cultures with glucose and mucus contained 2.25-fold
139 more CFU/mL on average than cultures without mucus (Fig. 1C). By the end of exponential
140 phase at 36h, we again recovered more viable cells from conditions with mucus, with 2.10-fold
141 more CFU/mL than without mucus. Without glucose, *C. difficile* exhibited a higher growth rate
142 during exponential phase with mucus (k = 0.142 ± 0.085 OD_{600}/hour) compared to the no-mucus
143 condition (k = 0.085±0.000 OD_{600}/hour) (Fig 1B). In addition, the presence of mucus increased
144 the number of viable cells; we recovered on average 2.68-fold more CFU/mL at 24h and 8.43-
145 fold more CFU/mL at 36h from cultures grown with mucus versus without (Fig. 1C). Altogether,
146 differences in optical density, growth rates, and CFU indicate mucus enhances *C. difficile*
147 growth, both when mucus supplements glucose and when mucus is the sole carbohydrate
148 source.
149 Because *C. difficile* exhibited increased growth in media with IEC-derived mucus, we
150 examined growth in co-culture with IECs with and without an intact mucus layer. The IECs were
151 stimulated to produce a robust mucus layer during differentiation as previously described (Fig.
152 1D, right)[27]. For controls without mucus, we removed the mucus layer and replaced it with PBS
153 (Fig. 1D, left). *C. difficile* was then inoculated at an MOI ~0.01. After 2h in co-culture, we
154 observed 14.0-fold greater expansion in CFU in co-cultures where the mucus layer was intact

155 compared to those without mucus (Fig. 1E). Overall, our results indicate that IEC-derived mucus
156 promotes *C. difficile* growth, both in broth and in the context of an infection model.

157 **Transcriptional profiling suggests mucus alters expression of genes with roles in**
158 **metabolism and nutrient acquisition**

159 To determine how *C. difficile* responds to the IEC-derived mucus, we used RNA-seq to
160 assess transcription in exponential-phase cultures grown with and without 50 μg/mL mucus in
161 CDMM. Because we were most interested in responses to mucus as opposed to stress or
162 starvation, 1% glucose was retained in the media. We identified 282 upregulated and 285
163 downregulated genes in the presence of mucus (567 total; fold change > 2, p-adj < 0.05) (File
164 S2, Fig. 2A). Among the five genes most upregulated in mucus, three are potential transporters
165 (CDR0455, CDR1626, and CDR2495), one is annotated as a TetR transcriptional regulator
166 (CDR0508), and one is annotated as a putative xanthine/uracil permease (CDR2014). The five
167 most downregulated genes are largely annotated as putative or hypothetical proteins, with one
168 probable protease (CDR3145). Principal components analysis indicated that mucus was the
169 main variable contributing to variance in the dataset (Figure 2B).

170 We next used gene set enrichment analysis (GSEA) to identify KEGG pathways
171 enriched in each condition. Using GSEAPreranked with all genes in *C. difficile*, we identified four
172 gene sets enriched with mucus and seven enriched without mucus (Fig. 2C, File S3). We further
173 refined these results using GSEAPreranked with the 567 most differentially expressed genes.
174 This analysis identified no gene sets significantly enriched in conditions without mucus; with
175 mucus, only the fructose and mannose metabolism pathway remained enriched (nominal p =
176 0.049, FDR q = 0.197). Figure 2D shows relative expression of highly differentially expressed
177 genes in this gene set. Among the seven genes contributing to core enrichment, five are
178 annotated as phosphotransferase system (PTS) components, which are important for sugar
179 uptake (Table S1). Specifically, CDR0692-0696 are involved in the transport of sorbitol, a host-
180 and diet-derived metabolite[30], while CDR2904 likely encodes part of a mannose PTS. These

181 analyses suggest mucus alters sugar uptake and metabolism in *C. difficile*, which prompted us
182 to search for additional genes that could play a role in utilizing nutrients from mucus.
183 Increased proportions of amino acids in the gut can lead to increased susceptibility for
184 CDI[31], with Stickland metabolism playing a key role in the conversion of amino acids for
185 growth[32]. Proline and glycine are particularly important for reductive Stickland metabolism, in
186 which proline and glycine reductases (PR and GR, respectively) are used to regenerate
187 NAD+[33]. Our analysis showed that all but three of the 19 genes within PR and GR clusters were
188 significantly downregulated with mucus (Table S1), suggesting that Stickland reduction of
189 proline and glycine is suppressed by *C. difficile* during mid-exponential phase when mucus is
190 present.
191 Recent work has revealed the importance of the Wood-Ljungdahl pathway (WLP), which
192 provides metabolic flexibility to *C. difficile* and potential advantages during infection[34,35].
193 Expression of WLP genes tends to be inversely correlated with PR and GR[36], and increased
194 expression of WLP genes could indicate an abundance of Stickland electron donors, such as
195 alanine, valine, serine, isoleucine, threonine, or glutamic acid[36,37]. Under such conditions,
196 alternative mechanisms of reduction are needed[36]. Given apparent inhibition of PR and GR by
197 mucus, we investigated WLP gene expression. Of 38 genes that have been previously identified
198 as part of the WLP or a linked glycine cleavage system (GCS, explained below) in *C. difficile*, 19
199 were upregulated and 15 were downregulated with mucus (p-adj < 0.05, File S2). We observed
200 increased expression of genes corresponding to branches of the WLP that fix CO_2 and convert it
201 to acetyl-CoA (Table S1). Upregulated genes encoding enzymes in these branches included: *fdh*
202 and *hyd* genes for reversible conversion between formate and CO_2; *metV* and *metF* encoding
203 components of N^5,N^{10}-methylene-tetrahydrofolate reductase, *cooS* for fixation of CO_2 via CO
204 dehydrogenase; and homologs of *acsE, acsC, acsD*, and *acsB*, which encode components of
205 acetyl-CoA synthase. WLP genes downregulated in mucus corresponded to interconversions
206 between acetyl-CoA and acetate, butyrate, or ethanol. These included homologs of *pta* and *ptb*,

207 encoding enzymes that convert between acetyl-CoA and acetylphosphate, as well as *ackA* and
208 *buk* for conversion between acetylphosphate and acetate. We also observed downregulation of
209 *thlA, hbd, crt2,* and *bcd-etfAB* homologs for conversion of acetyl-CoA to butyrate, and of *adhE*,
210 for conversion of acetyl-CoA to ethanol via acetaldehyde.

211 Linked to the WLP is a reversible glycine cleavage system (GCS) that provides
212 additional options for carbon assimilation in *C. difficile*[36,38]. We observed increased expression
213 of *gcvH* and *gcvL*, and decreased expression of *gcvP* and *gcvT*, which encode components of
214 the glycine cleavage reaction complex[39,40] (Table S1). Expression of *glyA,* which encodes a
215 serine/glycine hydroxymethyltransferase to interconvert glycine and serine, was also increased.
216 In addition, *sdaB,* which encodes a serine dehydratase that produces pyruvate from serine, was
217 upregulated. Overall, the presence of mucus decreased expression of PR and GR gene
218 clusters, but increased expression of genes related to CO_2 fixation via the WLP and glycine and
219 serine catabolism via the GCS.

220 **Mechanisms for transcriptional control are differentially expressed with mucus**

221 An abundance of genes for transcriptional regulation and responding to environmental
222 stimuli were differentially expressed (File S2), suggesting *C. difficile* senses mucus. Of highly
223 differentially expressed genes with fold change > 2 (Table S2), many are annotated to encode
224 transcriptional regulators, sigma factors, or antiterminators. Genes encoding transcriptional
225 regulators from the GntR family were most prevalent, and genes annotated as members of the
226 TetR, MarR, AraC, and MerR regulator families were also differentially expressed. These
227 families can regulate many cellular processes, including overall metabolism of carbon and
228 nitrogen (GntR, AraC), stress responses (TetR, AraC), and resistance to antibiotics, metals, or
229 other toxins (MarR, MerR)[41].

230 Two-component systems play a critical role in sensing and responding to environmental
231 stimuli. Among TCS genes (Table S2), CDR1568-1569 were upregulated, while CDR2206-2205,
232 *hexRK*, CDR2021-2020, and CDR2188-2187 were downregulated. Based on work in *C. difficile*

233 and with orthologous genes in *B. subtilis*, CDR1568-1569 could be involved in maintaining cell
234 surface homeostasis[42], while *hexRK*, and potentially CDR2021-2020, are involved in antibiotic
235 sensing and resistance[43,44]. Altogether, our data suggest mucus is an important stimulus for *C.*
236 *difficile,* perhaps indicating increased nutrient availability or proximity to the epithelium.

237 **Mutants lacking upregulated genes exhibited altered growth phenotypes with mucus.**

238 Among the genes most highly upregulated in *C. difficile* grown with mucus, we identified
239 several predicted to be involved in transport. CDR0455 and CDR2495 were among the five
240 most upregulated genes in mucus (Fig. 2A). CDR0455 forms a predicted operon with CDR0454-
241 0453, which were also significantly upregulated (Fig. 3A, File S2). Based on analyses of protein
242 homology in Phyre2[45], the operon likely encodes three membrane proteins consisting of an
243 endopeptidase (CDR0453), Na^+/H^+ antiporter (CDR0454), and transport protein (CDR0455).
244 CDR2495 encodes a membrane protein with homology to *E. coli* GadC, indicating potential
245 function in glutamate/γ-aminobutyrate exchange. GSEA identified upregulated PTS components
246 within the fructose and mannose metabolism gene set (Figure 2C, 2D, Table S1). Several of
247 these genes belong to a predicted operon encoding a sorbitol PTS encompassing *gutM, gutA,*
248 *srlE* (CDR0693)*, srlE', srlB,* and *gutD*, all of which were significantly upregulated in mucus (Fig.
249 3A, Table S1). Using qRT-PCR, we independently confirmed increased expression of CDR0455,
250 CDR0693, and CDR2495 under conditions used in the RNA-Seq experiment (Fig. S1). Given
251 consistent upregulation of these genes and their potential role as transporters, we predicted that
252 deletions in these genes would result in reduced growth in mucus. Thus, we generated in-frame
253 gene and operon deletions in *C. difficile* R20291: Δ0453-0455, Δ0693-0696, and Δ2495.

254 We evaluated growth of the mutants in CDMM containing 1% glucose with or without 50
255 μg/mL mucus (Fig. 3B). Like wildtype, all mutants had higher growth rates with mucus than
256 without (Fig. 3C). While wildtype and mutants showed similar growth in the absence of mucus,
257 unexpectedly, the Δ0693-0696 and Δ2495 mutants had significantly higher growth rates relative
258 to wildtype in mucus. Furthermore, after 24h Δ0453-0455 and Δ0693-0696 had 2.99-fold and

259 3.24-fold more CFU/mL with mucus, relative to respective growth without mucus (Fig. 3D). We
260 observed similar, albeit statistically insignificant, trends with wildtype and Δ2495 in mucus. In
261 media lacking glucose, we again observed that all strains had significantly more growth overall
262 with mucus than without mucus based on OD_{600} measurements and CFU at 24h (Fig. S2A-C).
263 However, in the absence of glucose, mucus did not significantly alter growth rates for any strain
264 (Fig. S2D), and the increased growth rates and shorter lag phases of mutants in conditions with
265 glucose were not observed.

266 To assess growth phenotypes in a native mucus layer, we evaluated the growth of each
267 mutant in co-culture with IECs and an intact mucus layer. After 6h co-culture, we observed at
268 least one log of growth for all strains (Fig. 3E). Consistent with results from broth culture
269 experiments, the mutants tended toward more growth relative to wildtype, with significantly
270 greater growth of Δ2495 (6.17-fold more CFU/mL for Δ2495 vs. wildtype; Fig. 3E). Altogether,
271 mutations in the selected genes and operons did not lead to growth defects in mucus as we
272 predicted, but instead resulted in greater growth than wildtype under these conditions.

273 ***C. difficile* biofilm formation may increase viscosity of *ex vivo* mucus.**

274 To evaluate the extent to which *C. difficile* can manipulate mucus, we performed
275 biophysical and biochemical analyses on native *ex vivo* mucus incubated for 24 hours with and
276 without *C. difficile*. Importantly, *C. difficile* remained viable and expanded within *ex vivo* mucus
277 (Fig. S3A). We applied particle tracking microrheology (PTMR) to measure the viscosity *C.*
278 *difficile*- and mock-inoculated mucus, using a Gaussian mixture model to distinguish watery
279 (less viscous) vs. mucoid (more viscous) fractions of mucus[28,46–48]. After 24 hours, mucus
280 containing *C. difficile* had more mucoid signal relative to the mock-inoculated control, as
281 indicated by increased detection of microbeads within the mucoid vs. watery fraction (Fig. 4A,
282 4C). This increased mucoid fraction corresponded to greater complex viscosity in samples
283 containing *C. difficile* relative to the mock-inoculated control (Fig. 4B). Multiangle laser light
284 scattering (MALLS), which measures mucin molecular weight, radius of gyration, and

285 concentration, indicated no changes in these metrics between inoculated and mock-inoculated
286 samples after 24h (Fig S3B-D).

287 While results indicate that *C. difficile* does not break down mucins sufficiently to detect
288 decreased molecular weights, the observed increase in viscosity could reflect additional ways *C.*
289 *difficile* responds to mucus. Biofilm formation within mucus can lead to increased viscosity, as
290 observed with *Pseudomonas aeruginosa*[48]. We therefore examined the impact of mucus on *C.*
291 *difficile* biofilm formation *in vitro*. We detected significantly greater biofilm biomass for *C. difficile*
292 grown with mucus versus without mucus (Fig. 4D), indicating that mucus promotes biofilm
293 formation, which may contribute to the increased viscosity we observed.

294 **Metabolic modeling predicts increased uptake of specific amino acids from mucus.**

295 To assess the metabolic potential of *C. difficile* during growth in mucus, we used
296 RIPTiDe to contextualize an established genome-scale metabolic network reconstruction
297 (GENRE) for *C. difficile* R20291 with our transcriptomic data[49–51]. To recapitulate conditions from
298 the RNA-Seq experiment, we allowed the model to use mucin-derived monosaccharides for
299 conditions with mucus and excluded them from the no-mucus condition. Ordination analyses
300 revealed that predicted core metabolic activity was distinct between conditions with and without
301 mucus (Fig. 5A). These differences in metabolic activity corresponded to a predicted 52.6%
302 increase in biomass flux, a proxy for growth rate, in conditions with mucus versus without (Fig.
303 5B). Overall, comparing biomass fluxes to experimental data (Fig. 1, 3) suggests the model
304 accurately predicted growth trends given respective transcriptomic contexts.

305 To rank relative importance of reactions in contributing to predicted differences in
306 biomass, we used a Random Forests classifier to determine mean decrease accuracies (MDA)
307 (Fig. 5C). The positive or negative median flux values shown indicate directionality of each
308 reaction. The first two reactions, corresponding to glycine hydroxymethyltransferase (GHMT)
309 and glycine synthase, are involved in the GCS. Negative flux values for GHMT indicated
310 conversion from serine to glycine in the mucus condition, while flux in the opposite direction was

311 predicted without mucus. Negative flux for glycine synthase also indicated biosynthesis of
312 glycine from 5,10-methylenetetrahydrofolate, which simultaneously generates NAD+, in the
313 presence of mucus. NADPH:oxidized-thioredoxin oxidoreductase and L-Glu:NAD+
314 oxidoreductase are also involved in redox chemistry. In the presence of mucus, positive flux
315 indicated oxidation of NADPH and reduction of thioredoxin was predicted for the former, and
316 negative flux indicated oxidation of NADH and reduction of 2-oxoglutarate to L-glutamate was
317 predicted for the latter. These results suggest glycine biosynthesis and regeneration of electron
318 carriers is important in the presence of mucus.

319 Reactions converting or transporting GlcNAc were also among the most important.
320 GlcNAc is a mucin-derived monosaccharide that can stimulate biofilm formation in *C. difficile*[52],
321 and is a component of biofilms[50,53]. For GlcNAc-1-phosphate 1,6-phosphomutase, negative flux
322 values with mucus indicated conversion from GlcNAc-1-phosphate to GlcNAc-6-phosphate (Fig.
323 5C). For GlcNAc transport, negative flux values, which were 8.42-fold greater with mucus than
324 without, indicated conversion of GlcNAc-6-phosphate to GlcNAc. Direct analysis of GlcNAc
325 exchange suggested that GlcNAc efflux was due to flux through the above reactions, with 5.16-
326 fold greater efflux with mucus than without (Fig. 5D).

327 Because glycine and serine are involved in reactions with the greatest MDA, we
328 examined predicted uptake for these amino acids. Glycine exchange was predicted to be
329 negligible in both conditions. Serine uptake, however, was predicted only in conditions with
330 mucus (Fig. 5E). This result makes sense considering flux through GHMT predicted
331 biosynthesis of glycine from serine in conditions with mucus, whereas without mucus, opposite
332 flux toward serine biosynthesis was predicted. As mucins are proline-, threonine-, and serine-
333 rich, we also examined predicted uptake of proline and threonine. We observed 1.53-fold
334 greater threonine uptake with mucus versus without. However, we observed the opposite trend
335 for proline uptake, with 29.4-fold more uptake predicted for the no-mucus condition versus with
336 mucus. These results coincide with RNA-Seq data suggesting proline metabolism via PR is less

337 active with mucus. Nonetheless, predicted increases in threonine and serine uptake in mucus
338 are intriguing as glycans are attached to mucins at serine and threonine residues.

339 **Mucus restores growth in defined media lacking specific amino acids.**

340 Metabolic modeling predicted glycine and serine interconversion to be particularly
341 important for differentiating growth with versus without mucus, and also predicted greater
342 uptake of serine and threonine from conditions with mucus. Hence, we experimentally
343 investigated the importance of these amino acids using DCAMM, a modified version of CDMM
344 with defined amino acid composition. We assessed growth with and without mucus in media
345 containing all amino acids (complete), lacking threonine (-T), or lacking serine (-S). Due to
346 interconversion of glycine and serine, we also assessed media lacking glycine (-G) or lacking
347 glycine and serine (-G -S). Importantly, complete DCAMM supported *C. difficile* growth
348 comparably to CDMM, with similar patterns of growth, including higher growth rates and more
349 CFU/mL at exponential phase, with versus without mucus (Fig. 1, 3, 6).

350 Removing threonine from the medium did not affect growth, but addition of mucus to -T
351 media promoted growth overall relative to conditions without mucus, as indicated by slightly
352 faster exits from lag phase (Fig. 6A) and increased growth rates (0.255±0.074 OD_{600}/h with
353 mucus vs. 0.217±0.018 without, Fig. 6D). However, we did not observe changes in CFU
354 between conditions with and without mucus in -T media at mid-exponential phase (Fig. 6C).

355 Conditions lacking both glycine and serine resulted in significant growth defects,
356 particularly a prolonged lag phase (Fig. 6A, 6B). Addition of mucus to -G -S medium enhanced
357 growth (Fig. 6B), yielding 24.3-fold more CFU/mL than -G -S medium without mucus (Fig 6C).
358 Growth rates between the two conditions were similar (Fig. 6D). Overall, a lack of glycine and
359 serine lengthened lag phase, and addition of mucus partially ameliorated this effect (Fig. 6B).

360 Cultures in -S medium without mucus also took longer to exit lag phase relative to -S
361 medium with mucus (Fig. 6A, 6B). Similar to -G -S conditions, addition of mucus increased
362 growth such that curves appeared more similar to those from complete media with mucus (Fig.

363 6B). In addition, growth in -S media with mucus yielded 3.65-fold more CFU/mL with mucus
364 versus without (Fig. 6C). In contrast, growth in -G media largely matched that in complete media
365 (Fig. 6A, 6B), with 1.74-fold more CFU/mL and significantly increased growth rates with mucus
366 compared to no mucus (k = 0.219±0.026 vs. 0.131±0.004 OD_{600}/h) (Fig. 6C, 6D). Together,
367 these results indicate that lack of serine has a greater impact on *C. difficile* growth than glycine
368 in the absence of mucus and suggests mucus serves as a source of serine.
369

370 **DISCUSSION**

371 In this study, we demonstrated that mucus derived from primary human IECs enhances
372 *C. difficile* growth and produces a variety of responses in the pathogen, particularly changes in
373 metabolism. These changes emphasize the metabolic plasticity and complexity of *C. difficile* in
374 its adaptive responses to mucus, which may involve differential sensing and transcriptional
375 regulation. Conversely, induction of biofilm formation by *C. difficile* may impact the viscoelastic
376 properties of mucus, which has ramifications for persistence.

377 Prior work examining the ability of *C. difficile* to utilize mucus as a nutrient source
378 indicated that other bacterial species are needed to liberate moieties from mucus. Our finding
379 that a low concentration of mucus produced a consistent, albeit subtle, increase in growth
380 indicates *C. difficile* can metabolize mucus independently. Indeed, this concentration was even
381 sufficient to elicit dramatic shifts in gene expression. Nonetheless, it remains likely that
382 contributions from other species *in vivo* enhances the use of mucus as a growth substrate.
383 Distinct properties of the mucus models used may have contributed to these different outcomes.
384 Prior work employed mucus from commercialized sources and immortalized cell lines and
385 applied a purification process resulting in a mono-component mucus containing a single mucin
386 type (MUC2)[20,23]. In contrast, our strategy was to remove free sugars and nutrients while
387 retaining as many features of native mucus as possible. Thus, the mucus we used to

388 supplement media would have retained more of the components and mucin types of native
389 colonic mucus, better reflecting nutrient availability in the colon.
390 In the presence of mucus, we observed increased expression of genes contributing to
391 CO_2 fixation via the WLP, and of genes encoding enzymes within the GCS, which is linked to the
392 WLP via methylene-THF (Fig. 7). The WLP may be particularly important later in infection, such
393 as when electron acceptors for Stickland metabolism are low[54]. However, others have reasoned
394 that the WLP remains important under heterotrophic conditions to allow utilization of CO_2
395 produced during glycolysis[35]. Metabolic modeling emphasized the importance of the GCS and
396 the conversion of serine to glycine in the presence of mucus (Fig. 7), as predicted fluxes from
397 the GCS and from GHMT indicate that glycine biosynthesis is particularly important. Glycine is a
398 key electron acceptor in Stickland metabolism, where it is reduced to acetylphosphate via
399 GR[33,34]. We observed reduced expression of GR with mucus, suggesting alternative
400 mechanisms for glycine metabolism under the conditions tested.
401 Serine also appears to be important during growth in mucus. Metabolic models predicted
402 uptake of serine only when mucus is present and a role for serine in glycine biosynthesis via
403 GHMT. Consistent with this prediction, the growth defect observed in DCAMM lacking serine
404 was improved by adding mucus, suggesting that mucus is a source of serine for *C. difficile*.
405 Importantly, serine deamination is one of the largest contributors to the pyruvate pool in *C.*
406 *difficile*[36] (Fig. 7), thus influencing glycolysis, the TCA cycle, and the WLP[34]. In addition,
407 pyruvate fermentation is linked to toxin repression[55,56], so an increase in serine uptake from
408 mucus has potential ramifications for *C. difficile* pathogenesis. Overall, serine and glycine likely
409 contribute synergistically to the flexibility of *C. difficile* metabolism and its growth.
410 Experimental data and metabolic modeling suggest that mucus stimulates biofilm
411 formation (Fig. 7). *C. difficile* has been demonstrated to form biofilms on purified MUC2,
412 particularly in co-culture with *Fusobacterium nucleatum*[13], suggesting *C. difficile* can form
413 biofilms in the human colon. Several biofilm-related genes, such as those involved in GlcNAc

414 biosynthesis[57,58] and polysaccharide II synthesis and export[59], were upregulated in the mucus
415 condition (File S2). In line with these data, metabolic modeling predicted the efflux of GlcNAc, a
416 component of biofilm polysaccharides from various organisms[60–63]. Furthermore, when provided
417 alongside pyruvate, GlcNAc promotes biofilm formation[52]. Past work in *B. subtilis* indicated
418 GlcNAc export was enhanced by manipulating features of glucose metabolism[64]; we can thus
419 speculate that alterations to *C. difficile* metabolism may promote the GlcNAc efflux predicted by
420 modeling (Fig. 7). Others have noted increased production of proteins from the WLP and GCS
421 in some biofilm models[65], indicating that there are several potential connections between *C.*
422 *difficile* metabolic activity and mucus-induced biofilm formation.

423 Biophysical and biochemical analyses did not demonstrate substantive breakdown of
424 mucins by *C. difficile* independently, which fits prior evidence that multiple species working in
425 concert are required for efficient degradation of mucins[20,66,67]. Nonetheless, given the repertoire
426 of carbohydrate-active enzymes in *C. difficile* R20291[21], activity may exist to cleave glycans or
427 other fragments from mucus without producing detectable differences in molecular weight.
428 Indeed, we observed significant upregulation of 31 of the 72 CAZy genes in *C. difficile* (File S2),
429 including enzymes with potential mucolytic activity[20,68,69].

430 Many genes related to transcriptional regulation and signal transduction were
431 differentially expressed in response to mucus. In a past study looking at the transcriptional
432 response of *Pseudomonas aeruginosa* to mucus-supplemented media[70], researchers concluded
433 that selection for specific regulatory and signaling mechanisms likely led to the differential
434 expression of metabolism-related genes they observed with mucus. The differential expression
435 of transcriptional regulators in our dataset could contribute to the phenotypic and metabolic
436 changes we observed with mucus, but further exploration into these mechanisms is needed.

437 Finally, deleting genes upregulated during growth in mucus, which included genes with
438 predicted roles in sugar uptake or transport, did not lead to growth defects in mucus. Instead,
439 mutants exhibited growth that exceeded that of wildtype. These unexpected growth phenotypes

440 could be related to tradeoffs in adaptation to versus growth in mucus. The identification of many
441 differentially expressed genes related to transcriptional control and signal transduction supports
442 a role for mucus as a stimulus to alter *C. difficile* metabolism, and indeed, mucin glycans have
443 been widely demonstrated to stimulate shifts in microbial gene expression and behavior[71].
444 Moreover, it has been posited that a greater capacity to sense multiple nutrients in an
445 environment is metabolically costly, contributing to longer lag phases[72]. Under these
446 assumptions, inefficiencies in sensing, as might be expected for strains lacking transporters[73],
447 could result in shorter lag phases but incur other long-term fitness costs. Further analysis for
448 gene essentiality may identify mechanisms *C. difficile* relies on in its interactions with mucus.
449 Overall, our data support a model in which colonic mucus promotes *C. difficile* growth as
450 a source of specific amino acids and a likely source of carbohydrates, which could translate to
451 enhanced colonization *in vivo*. Alterations in expression observed with mucus highlight the
452 metabolic flexibility of *C. difficile*, which is likely a key factor for biofilm formation and persistence
453 in a dynamic host environment[35]. Importantly, biofilms are a main contributor to recurrence[74],
454 providing an environment protected from antibiotics and from which spores can be generated to
455 promote continued infection[75]. Our work demonstrates that *C. difficile* possesses mechanisms to
456 take advantage of this niche. In better understanding *C. difficile*-mucus interactions, more
457 effective therapeutics to disrupt colonization or promote mucosal immunity can be developed.
458

459 **MATERIALS AND METHODS**

460 **Bacterial strains and growth conditions.** Table S3 lists strains and plasmids used in this
461 study. *Clostridioides difficile* R20291 was routinely cultured in TY (3% w/v Bacto tryptone, 2%
462 w/v yeast extract, 0.1% w/v thioglycolate)[76], BHIS (3.7% w/v brain heart infusion, 0.5% w/v
463 yeast extract, 0.1% w/v cysteine)[76], *C. difficile* minimal medium (CDMM)[29], or CDMM with
464 defined amino acids (DCAMM, described below and in File S1) at 37°C in an anaerobic
465 chamber (Coy) with an atmosphere of 5% CO_2, 10% H_2, and 85% N_2. *E. coli* strains were grown

466 aerobically at 37°C in lysogeny broth (LB, Miller), and conjugations with *C. difficile* performed
467 anaerobically. Methods for cloning and *C. difficile* mutagenesis, as previously applied[77,78], are
468 detailed in Text S1. Preparation of *C. difficile* cultures for growth assays are detailed in Text S1.
469 **Primary human intestinal epithelial cell (IEC) cultures and generation of a mucus layer.** All
470 IECs were derived from the transverse colon of a 23-year-old male cadaveric donor. Cultures
471 were maintained in Sato's Expansion Medium (Sato's EM)[79]. Transwells (0.4 µm pore, PET,
472 Corning) were coated with 10 µg/mL collagen at least four hours prior to seeding cells in
473 Expansion Medium (EM). EM was replaced every other day until a confluent monolayer formed
474 (5-7 days, or until trans-epithelial electrical resistance measured ≥ 500 ohms x cm^2). To
475 generate a mucus layer, confluent monolayers were cultured in differentiation medium with 330
476 ng/mL vasoactive intestinal peptide (DM+VIP) in an air-liquid interface[27,28]. DM+VIP was
477 replaced daily. File S1 contains compositions of cell culture media.
478 ***Ex vivo* mucus purification.** After 4-5 days of differentiation, mucus was removed from the
479 apical surface of the IECs. Epithelia were rinsed with PBS to collect residual mucus. Collected
480 mucus and rinses were stored at -20°C prior to purification. Mucus samples were pooled and
481 filtered using nominal molecular weight limit membranes (Amicon Ultra 3K, Millipore Sigma) to
482 remove free nutrients, metabolites, and contaminants. This purified mucus was suspended in
483 PBS, and total mucus protein concentration was determined using Pierce™ BCA Protein Assay
484 (Thermo Fisher) for standardization[12]. For supplementing media, a relatively low standard
485 concentration of 50 µg/mL mucus was used due to limited availability of IEC-derived mucus.
486 ***C. difficile*-IEC co-cultures.** Mucus-producing IECs (4-5 days in DM+VIP) were used to assess
487 growth of *C. difficile* with or without a mucus barrier. Controls lacking mucus were prepared by
488 removing the mucus layer and rinsing epithelia three times with PBS. PBS was then added to
489 the apical compartment (100 µl, approximately the same volume as mucus). IECs were
490 transferred to an anaerobic chamber and inoculated with *C. difficile* (10^3 CFU, MOI ~0.01). To

491 recover *C. difficile* after co-culture, 0.1% DTT in PBS was added to each apical compartment,
492 then the plate was placed on a rocking platform for 20 minutes at room temperature break down
493 mucus. CFU in the apical compartment were enumerated by plating serial dilutions.
494 **RNA-sequencing.** Early stationary phase cultures in TY broth were pelleted and washed with
495 PBS, then inoculated into CDMM with or without 50 µg/mL mucus at an OD_{600} of 0.05. At
496 exponential phase (OD_{600} ~0.5), cultures were collected and RNA extracted using TriZol as
497 described[80], followed by purification and DNase treatment (RNeasy kit, RNase-Free DNase Set,
498 Qiagen). RNA was submitted for 150 bp paired-end sequencing on an Illumina HiSeq platform
499 (Azenta Life Sciences). Read processing, including quality assessment, filtering, and mapping
500 steps, were performed using established bioinformatic tools[81–83]. To perform genomic feature
501 counting, we used a prokaryote-specific algorithm, Feature Aggregate Depth Utility (FADU;
502 v1.8)[84]. After obtaining read counts per gene, we used DESeq2 (v1.42.0) in R for differential
503 expression analysis[85]. For Gene Set Enrichment Analysis (GSEA, v4.1.0)[86,87], we used
504 normalized counts from DESeq2 and gene sets from KEGG. We then used default ranking
505 metrics generated by GSEA to run GSEAPreranked and generate normalized enrichment
506 scores for each gene set. We also narrowed the list of genes applied to GSEAPreranked to only
507 those meeting a differential expression threshold (Benjamini-Hochberg corrected $p < 0.05$, fold
508 change > 2), using Log_2 fold change as the ranking metric. Select differentially expressed genes
509 were validated using qRT-PCR as previously described[78,88,89]. Text S1 contains further RNA
510 isolation, read processing, and qRT-PCR details.
511 ***Ex vivo* mucus preparation for biophysical and biochemical characterization.** Mucus was
512 collected and stored at -20°C, then pooled before use to achieve sufficient material. To the pool,
513 CDMM salts (final concentration in mucus 0.5X), trace salts (1X), iron sulfate heptahydrate (1X),
514 and vitamins (1X) (File S1) were added to provide minimally necessary components for
515 *C. difficile* survival. To ensure adequate mucus concentration (>2.5% solids), aliquots were dried
516 and percent solids determined by comparing initial aliquot weight to dry weight. To prepare *C.*

517 *difficile* inoculums, cultures were grown to exponential phase in CDMM with 50 µg/mL mucus,
518 then pelleted and washed with CDMM salts (1X) and trace salts (1X) (File S1, hereafter 1X
519 CDMM salts). Mucus samples were inoculated with 10^6 CFU *C. difficile* in 1X CDMM salts at a
520 1:20 dilution. To prepare controls lacking *C. difficile*, we mock-inoculated mucus with 1X CDMM
521 salts. Samples were collected at inoculation and 24 hours post-inoculation to confirm *C. difficile*
522 viability and for biophysical and biochemical analyses.
523 **Biophysical and biochemical analysis of *ex vivo* mucus.** Biophysical analysis using particle
524 tracking microrheology (PTMR) to determine complex viscosity of *ex vivo* mucus was performed
525 as described[28,90,91]. Biochemical analyses using multiangle laser light scattering (MALLS) to
526 measure mucin molecular weights, radii of gyration, and concentrations in *ex vivo* mucus were
527 also performed as described[28]. Specific details for each technique are in Text S1.
528 **Biofilm assays.** Overnight cultures of *C. difficile* grown in TY broth were pelleted and washed
529 with PBS, then diluted 1:30 in CDMM with or without 50 µg/mL mucus. Cultures were grown to
530 an OD_{600} 0.8-1, normalized toOD_{600} 0.5, and aliquoted into untreated 96-well polystyrene plates.
531 Assay methods were adapted from past work[92–94]; details are in Text S1.
532 **Context-specific metabolic modeling.** We contextualized a published *C. difficile* R20291
533 genome-scale metabolic network reconstruction (GENRE) for conditions with and without
534 mucus as described[49–51], using transcript per million values from the RNA-Seq experiment and
535 the maxfit_contextualize() function in RIPTiDe with default settings. The model was constrained
536 to fit minimal media conditions used (CDMM with or without mucus)[49]. Bray-Curtis dissimilarity,
537 nonmetric multidimensional scaling, and PERMANOVA statistical testing were performed using
538 the vegan R package (v.2.6-4)[50]. To determine reactions important for differentiating conditions,
539 supervised machine learning was performed using the randomForest R package (v. 4.7-1.1)[50].
540 Differences in predicted fluxes were determined using Wilcoxon rank sum test[50].
541 **Growth experiments with defined amino acids minimal medium (DCAMM)**. To test the
542 contribution of glycine, serine, or threonine to *C. difficile* growth while keeping conditions

543 consistent with prior experiments, we created a defined casein amino acids minimal medium
544 (DCAMM, File S1). To approximate relative proportions of each amino acid in 10 mg/mL
545 casamino acids (the concentration in CDMM), amino acid content for bovine casein (alpha-S1,
546 alpha-S2, and beta casein subunits, UniProt IDs P02662, P02663, P02666 respectively) was
547 used. All other components of DCAMM were unchanged. *C. difficile* growth curves in each
548 media with or without 50 µg/mL mucus were performed as described in Text S1.
549 **Data Availability.** Unless otherwise noted, all statistical analyses were performed using R
550 (v4.3.2) or GraphPad Prism 10. R, Python, and bash scripts for applying bioinformatic tools are
551 available from GitHub: https://github.com/klfurtado/2024_Cdiff_Mucus_Paper. RNA-Seq reads
552 are available from NCBI Gene Expression Omnibus (GSE254621).
553

554 **ACKNOWLEDGEMENTS**

555 This work was supported by NIH R01-DK120606 to RT and NLA; NIH R01-AI143638 to RT; and
556 NIH P30-DK065988 and Cystic Fibrosis Foundation HILL20Y2-OUT to DBH. NLA has a
557 financial interest in Altis Biosystems. We thank Kimberly Walker for her careful review of the
558 manuscript and Jilarie Santos Santiago for her assistance in maintaining IEC cultures.
559
560
561
562
563
564
565
566

567 **FIGURES**

568

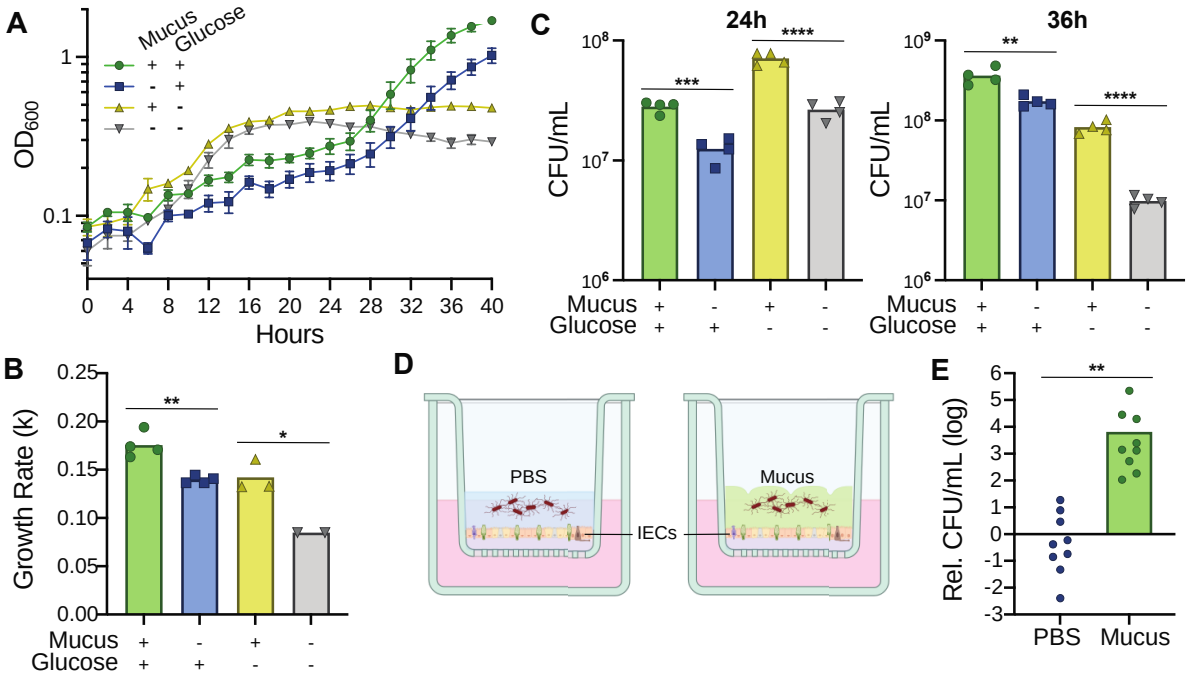

Figure 1. Mucus derived from primary human IECs enhances *C. difficile* growth. (A) *C. difficile* R20291 growth curves in CDMM containing purified mucus and glucose (+/+), glucose only (-/+), purified mucus only (+/-), or no mucus or glucose (-/-). Data are from one representative experiment, n=4. **(B)** Growth rates during exponential phase in each medium. Exponential phase was defined by having at least three time points in a linear range; samples for which at least three time points in a linear range could not be identified were excluded. **(C)** Viable cell counts expressed as CFU/mL after 24 hours (left) and 36 hours (right) growth in each medium. **(D)** Schematic of the primary human IEC co-culture system. IECs secrete produce a thick mucus barrier that can be inoculated with bacteria (right). As a control, the mucus layer was removed mechanically and replaced with PBS (left). **(E)** *C. difficile* viable cell counts after 2h co-culture with IECs. CFU/mL values were normalized to the CFU/mL present in the respective inoculum, then expressed relative to the mean normalized CFU/mL in the PBS condition. Data are from three independent experiments, n=3 per experiment. *$p < 0.05$, **$p < 0.01$, ***$p < 0.001$, ****$p < 0.0001$, unpaired, two-tailed t-test.

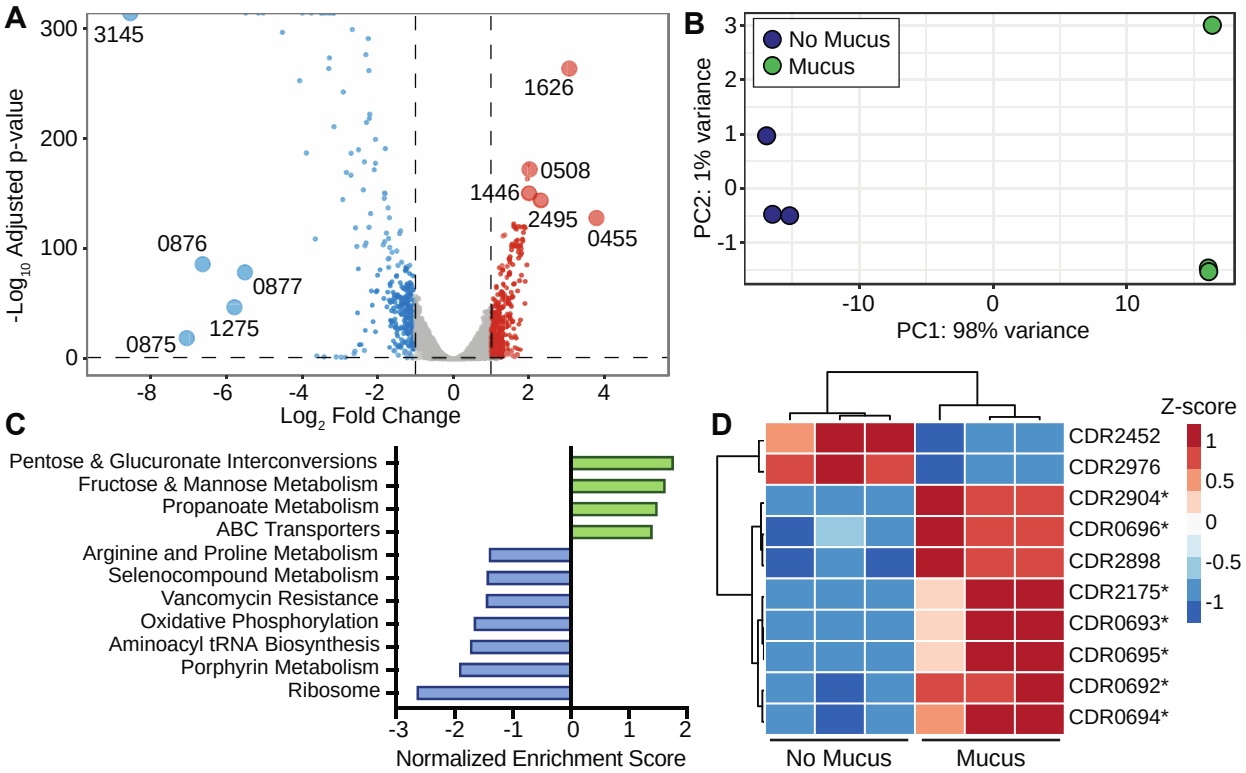

Figure 2. Mucus leads to a distinct and robust transcriptional response affecting metabolism. (A) Volcano plot highlighting all genes differentially expressed in CDMM with mucus vs. no mucus with Benjamini-Hochberg adjusted p-value < 0.05 and fold changes > 2 ($\log_2$ fold changes > 1 or < -1), based on Wald test in DESeq2. Genes significantly upregulated (red) and downregulated (blue) with mucus are shown. The 5 most upregulated and downregulated genes are labelled by the last 4 digits of their locus tag (CDR20291_XXXX, hereafter abbreviated as CDRXXXX). **(B)** PCA plot after variance stabilizing transformation of read counts in DESeq2, n=3 per condition. **(C)** Normalized enrichment scores for KEGG gene sets identified using GSEAPreranked considering relative expression all genes in *C. difficile* R20291. The selected gene sets were enriched in the presence (green) or absence (blue) of mucus, nominal p < 0.05 and/or FDR q-value < 0.25. **(D)** Heatmap of genes in the fructose and mannose metabolism gene set identified using GSEAPreranked based on genes with adjusted p < 0.05 and fold change > 2 from RNA-Seq. Starred genes contributed to core enrichment of the gene set.

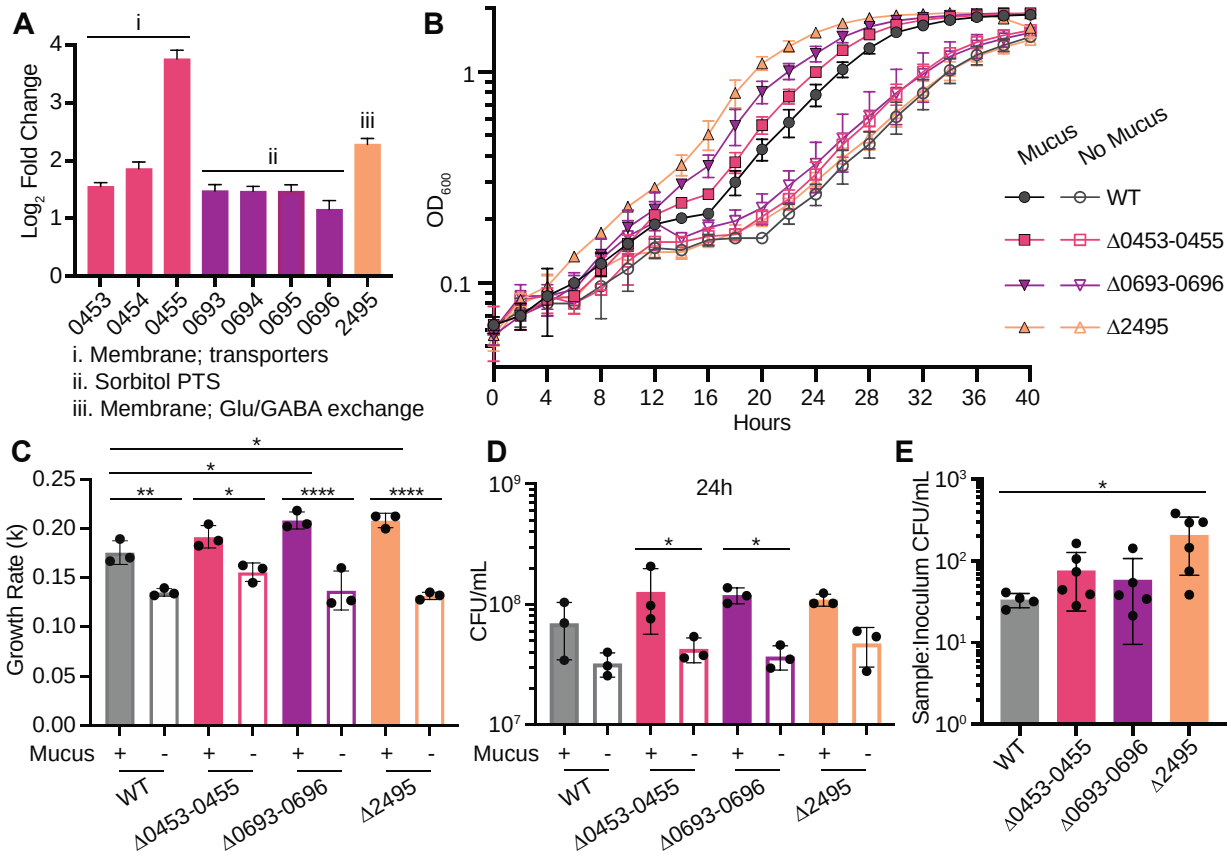

Figure 3. Deletion of genes and operons upregulated with mucus enhances growth. (A) Log_2 fold change expression values and standard error for genes and operons selected for mutagenesis. CDR0453-0455 and CDR2495 were among the most highly upregulated; CDR0693-0696 contributed to core enrichment of the fructose and mannose metabolism gene set in mucus (Fig 2). Predicted functions based on Phyre2 analysis or prior studies are indicated. **(B)** Growth curves for mutants and wildtype in CDMM with mucus (filled symbols) and without mucus (open symbols). Data are from one representative experiment, n=3. **(C)** Growth rates during exponential phase. **(D)** Viable cell counts expressed as CFU/mL. **(E)** Viable cell counts after 6h co-culture with IECs with an intact mucus barrier. Viable cell counts are expressed as CFU/mL in each sample after 6h, normalized to CFU/mL present in respective inoculum for each strain. Data are combined from two independent experiments, n=2 or 3 per experiment. Outliers were determined and removed using Grubbs' method. *$p < 0.05$, **$p < 0.01$, ***$p < 0.001$, ****$p < 0.0001$, one-way ANOVA with Tukey's or Sidak's tests

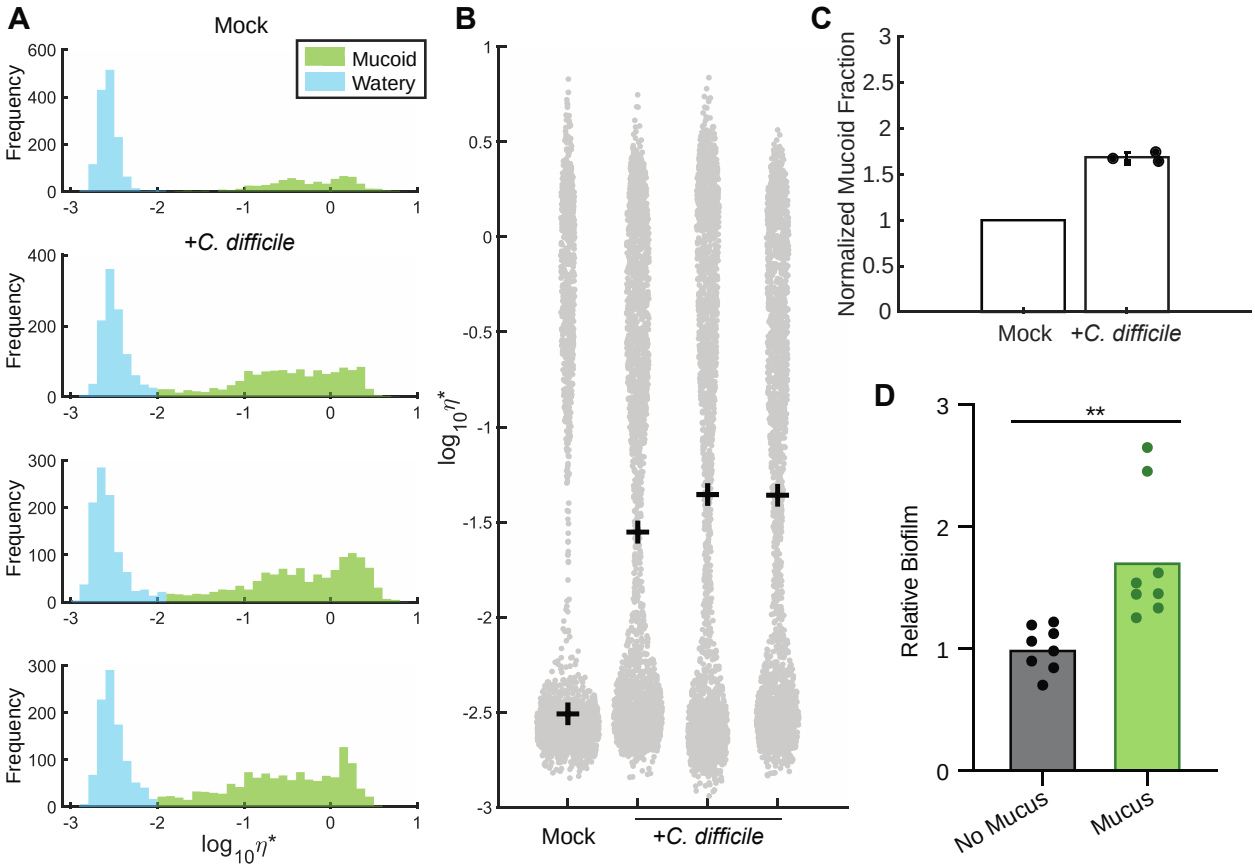

Figure 4. *C. difficile* increases viscosity of *ex vivo* mucus. (A) PTMR analysis of *ex vivo* IEC mucus inoculated with *C. difficile* or mock-inoculated with 1X CDMM salts. A Gaussian mixture model was employed to distinguish mucoid rheological behavior from that of watery mucus after 24 hours. An increasing frequency of detection of microbeads within the mucoid fraction is indicated by larger green peaks. **(B)** Complex viscosity (η*) of mucus-grown samples after 24h. Individual points represent measured complex viscosity from each microbead, and crosses represent mean η* per sample. **(C)** Quantified mucoid fractions in mucus inoculated with *C. difficile* relative to the mock-inoculated control based on PTMR data in (A) For each sample, three slides were prepared and 10 videos recorded per slide. **(D)** Biofilm formation by *C. difficile* in CDMM with or without mucus after 24h, expressed as absorbance at 570nm for each sample relative to mean absorbance of the no mucus condition. Data from 2 independent experiments, n=4 per experiment, were combined. **$p < 0.01$, unpaired two-tailed t-test.

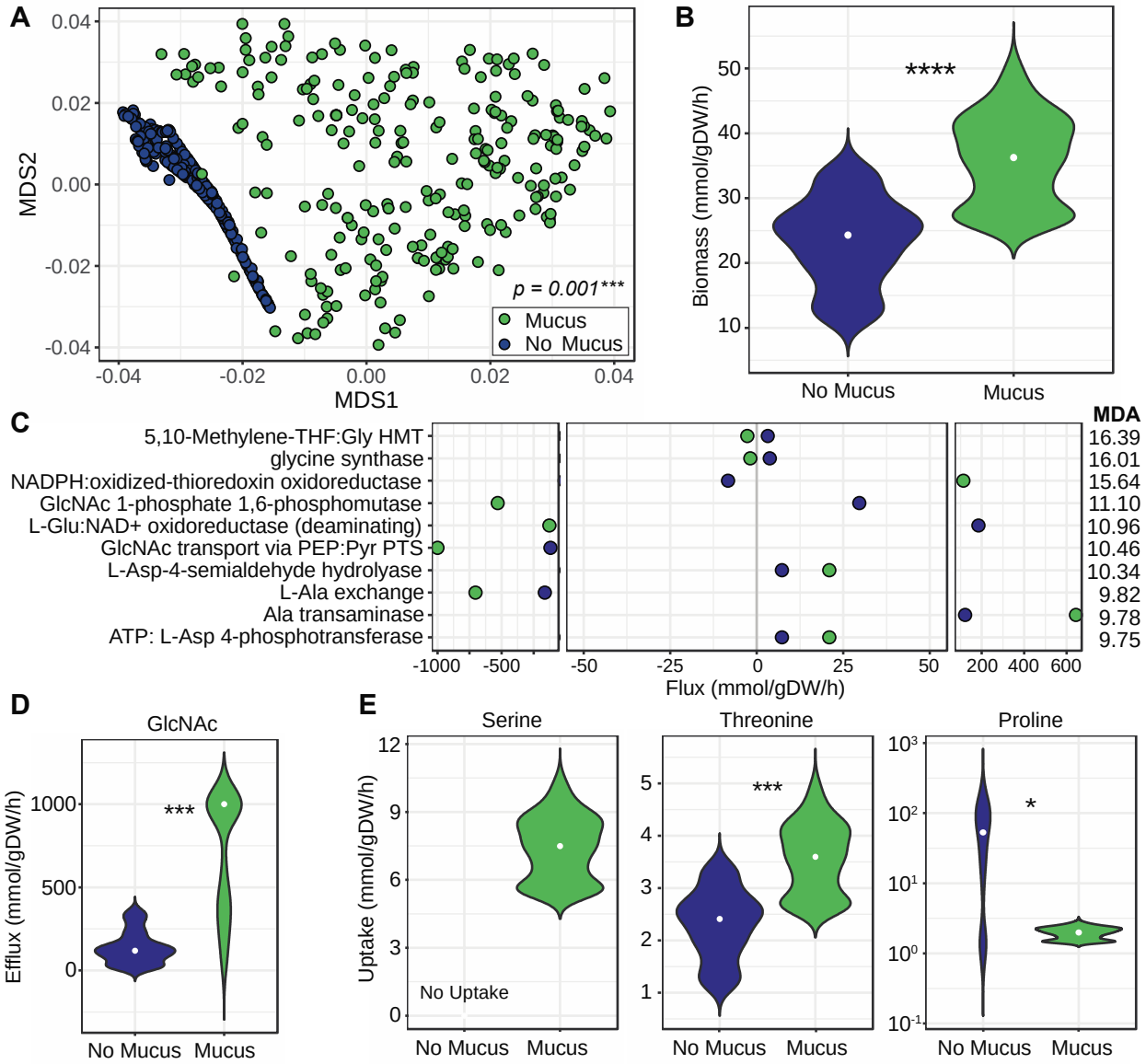

Figure 5. Modeled *C. difficile* growth predicts distinct metabolic activity in the presence of mucus. (A) Predicted core metabolic activity for *C. difficile* from conditions with vs. without mucus, using a *C. difficile* GENRE contextualized with transcriptomic data. Data are represented as NMDS ordination of the Bray-Curtis dissimilarity of flux distributions from shared reactions in each contextualized model. Differences between conditions were determined by PERMANOVA. (B) Predicted biomass flux in CDMM with vs. without mucus. (C) Median fluxes for reactions determined by Random Forests analysis to be important in differentiating conditions with (green) vs. without mucus (blue). Reactions are ranked by MDA with larger values indicating greater importance. (D) Predicted GlcNAc efflux in conditions with vs. without mucus. (E) Predicted uptake of the indicated amino acids in conditions vs. without mucus. Data were generated from n=250 samplings from each contextualized model. Median flux values in B, D, and E are indicated (white dot). Differences in B, D, and E were determined by measuring p-values from a Wilcoxon rank sum test based on n=12 random subsamples from each condition (5% of total samples). This random subsampling and testing process was repeated 1000 times and the median p-value was used: *$p < 0.05$, **$p < 0.01$, ***$p < 0.001$, ****$p < 0.0001$.

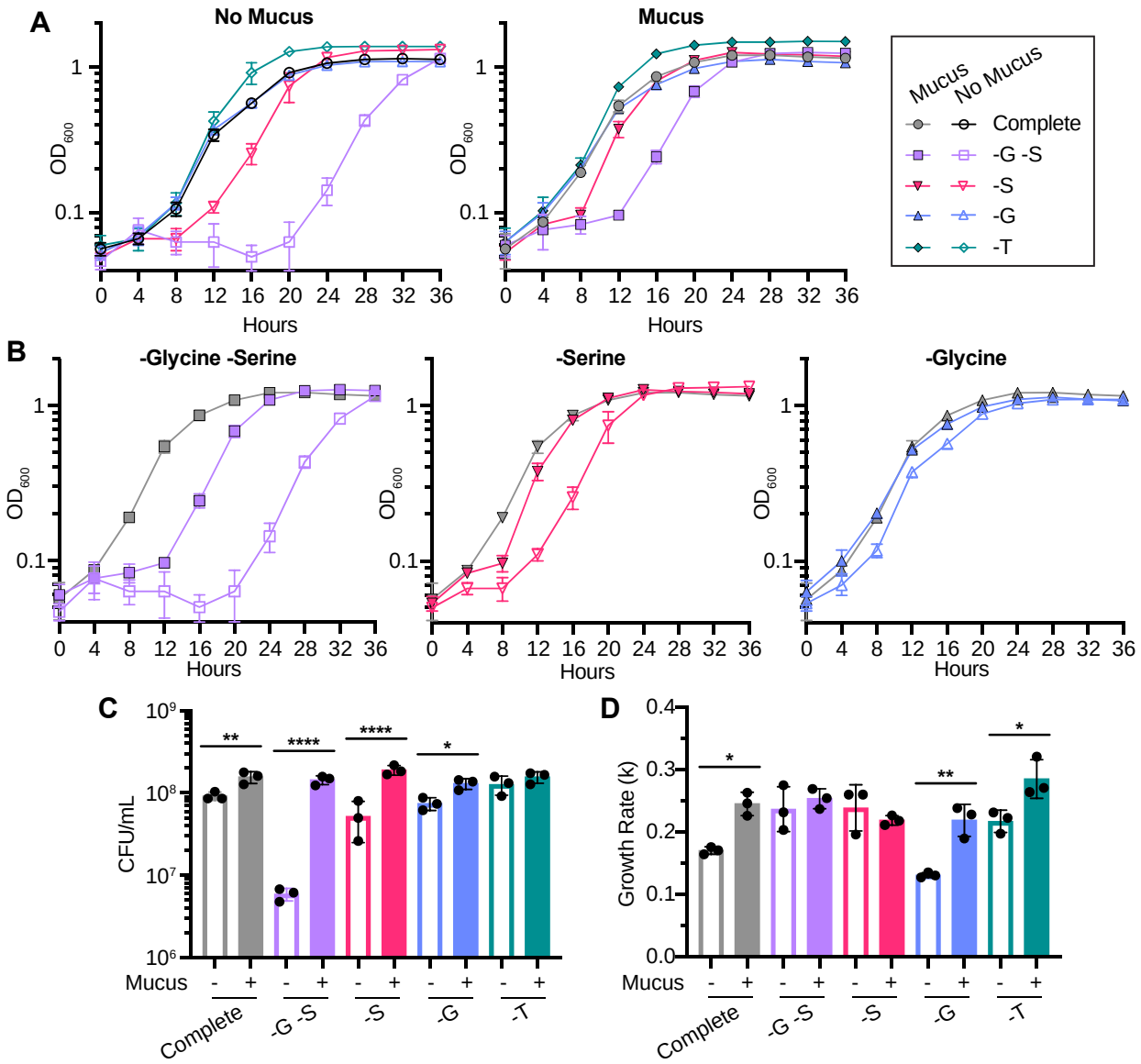

Figure 6. Mucus restores growth in media lacking specific amino acids. **(A)** *C. difficile* growth curves in a modified version of CDMM with defined casamino acids (DCAMM) without mucus (left) and with mucus (right), comparing growth between complete medium and media lacking specific amino acids. **(B)** Growth curves from (A) comparing growth with and without mucus (filled vs. open symbols) for specific conditions: lacking glycine and serine (left), lacking serine only (middle), and lacking glycine only (right). The growth curve from complete medium with mucus is shown on each graph for comparison (grey). (C) Viable cell counts (CFU/mL) at exponential phase. For each pair of media conditions with and without mucus, samples were collected when cultures for either condition first reached exponential phase (OD_{600} ~0.5), which occurred at: 12 hours for complete, -G, and -T media; 16 hours for -S medium; and 20 hours for -G -S medium. (D) Growth rates during exponential phase. * $p < 0.05$, ** $p < 0.01$, *** $p < 0.001$, **** $p < 0.0001$ determined by (C, D) one-way ANOVA with Sidak's test.

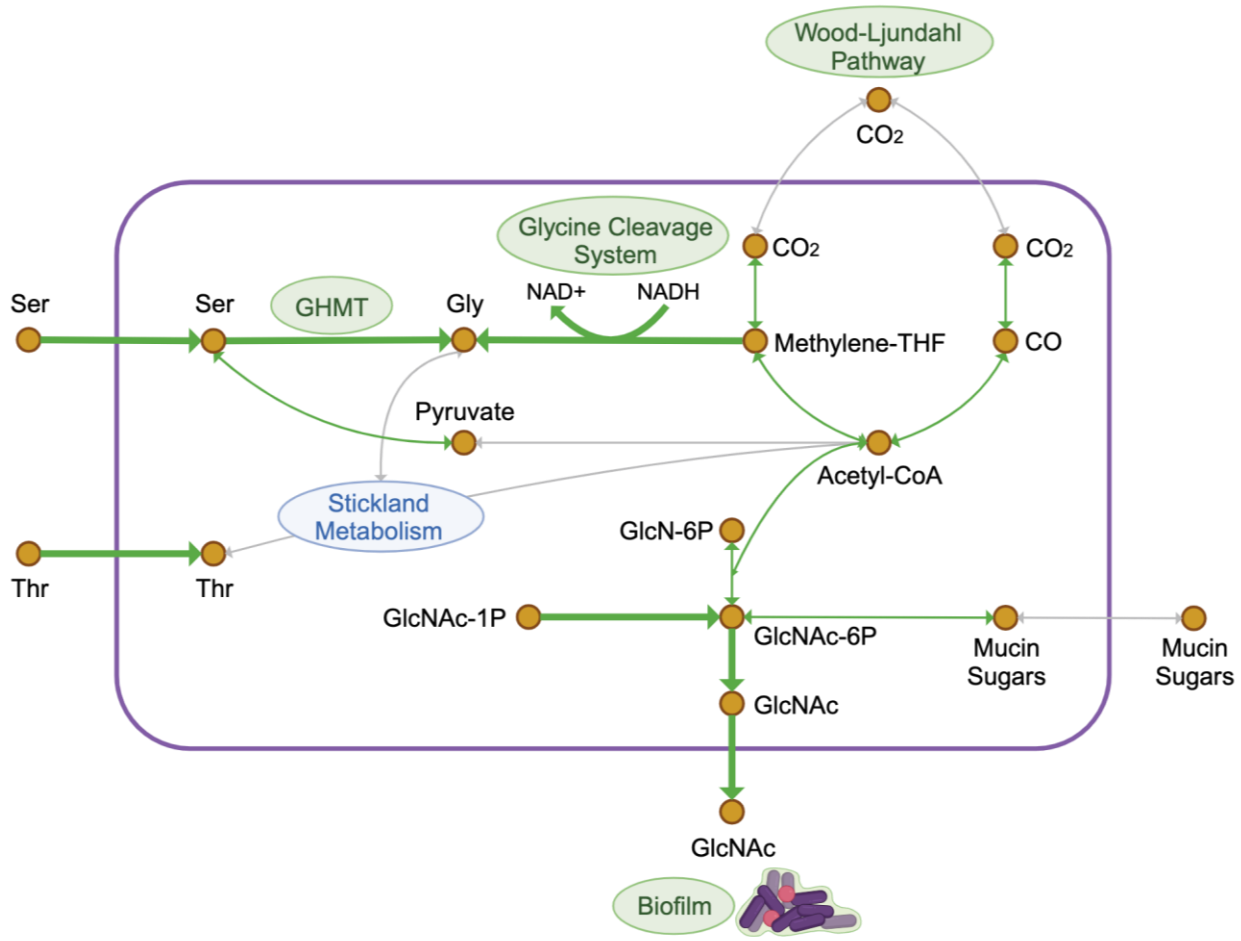

Figure 7. Overview of responses to IEC mucus in *C. difficile*. Simplified diagram of key reactions in the metabolic model and/or identified in the RNA-Seq experiment. Thicker green arrows indicate select reactions determined to be important in Random Forests analysis following contextualization of a *C. difficile* R20291 metabolic model; arrow directions indicate the direction of flux predicted with mucus. Paths within which we identified upregulation of genes corresponding to enzymes are identified with thin green lines. Abbreviations: Ser, serine; Thr, threonine; Gly, glycine; GHMT, glycine hydroxymethyltransferase; Methylene-THF, methylene-tetrahydrofolate; GlcN-6P, glucosamine-6-phosphate; GlcNAc, N-acetylglucosamine; GlcNAc-6P, N-acetylglucosamine-6-phosphate; GlcNAc-1P, N-acetylglucosamine-1-phosphate; CO_2, carbon dioxide; CO, carbon monoxide. Created with Biorender.com.

687 **REFERENCES:**

688 1. Centers for Disease Control and Prevention. Antibiotic Resistance Threats in the United
689 States, 2019. (2019) doi:10.15620/cdc:82532.
690 2. Eyre, D. W. *et al.* Predictors of first recurrence of *Clostridium difficile* infection:
691 Implications for initial management. *Clinical Infectious Diseases* **55**, (2012).
692 3. Merrigan, M. M. *et al.* Surface-layer protein A (SlpA) is a major contributor to host-cell
693 adherence of *Clostridium difficile*. *PLoS One* **8**, e78404 (2013).
694 4. Spigaglia, P. *et al.* Surface-layer (S-layer) of human and animal *Clostridium difficile*
695 strains and their behaviour in adherence to epithelial cells and intestinal colonization. *J*
696 *Med Microbiol* **62**, 1386–1393 (2013).
697 5. Baban, S. T. *et al.* The role of flagella in *Clostridium difficile* pathogenesis: Comparison
698 between a non-epidemic and an epidemic Strain. *PLoS One* **8**, (2013).
699 6. McKee, R. W., Aleksanyan, N., Garrett, E. M. & Tamayo, R. Type IV Pili promote
700 *Clostridium difficile* adherence and persistence in a mouse model of infection. *Infect*
701 *Immun* **86**, (2018).
702 7. Shen, A. *Clostridium difficile* toxins: Mediators of inflammation. *J Innate Immun* **4**, 149–
703 158 (2012).
704 8. Bacci, S., Mølbak, K., Kjeldsen, M. K. & Olsen, K. E. P. Binary toxin and death after
705 *Clostridium difficile* infection. *Emerg Infect Dis* **17**, 976–982 (2011).
706 9. Schwan, C. *et al. Clostridium difficile* toxin CDT induces formation of microtubule-based
707 protrusions and increases adherence of bacteria. *PLoS Pathog* **5**, e1000626 (2009).
708 10. McGuckin, M. A., Lindén, S. K., Sutton, P. & Florin, T. H. Mucin dynamics and enteric
709 pathogens. *Nat Rev Microbiol* **9**, 265–278 (2011).
710 11. Semenyuk, E. G. *et al.* Analysis of bacterial communities during *Clostridium difficile*
711 infection in the mouse. *Infect Immun* **83**, 4383–4391 (2015).
712 12. Engevik, M. A. *et al.* Human *Clostridium difficile* infection: altered mucus production and
713 composition. *American Journal of Physiology-Gastrointestinal and Liver Physiology* **308**,
714 G510–G524 (2015).
715 13. Engevik, M. A. *et al. Fusobacterium nucleatum* adheres to *Clostridioides difficile* via the
716 RadD adhesin to enhance biofilm formation in intestinal mucus. *Gastroenterology* **160**,
717 1301-1314.e8 (2021).
718 14. Arike, L. & Hansson, G. C. The densely O-glycosylated MUC2 mucin protects the
719 intestine and provides food for the commensal bacteria. *J Mol Biol* **428**, 3221-3229
720 (2016).
721 15. Parry, S. *et al.* N-Glycosylation of the MUC1 mucin in epithelial cells and secretions.
722 *Glycobiology* **16**, 623–634 (2006).
723 16. Johansson, M. E. V., Holmén Larsson, J. M. & Hansson, G. C. The two mucus layers of
724 colon are organized by the MUC2 mucin, whereas the outer layer is a legislator of host-
725 microbial interactions. *Proc Natl Acad Sci USA* **108**, 4659–4665 (2011).
726 17. Hanisch, F.-G. & Müller, S. MUC1: The polymorphic appearance of a human mucin.
727 *Glycobiology* **10**, 439-449 (2000).
728 18. Lang, T., Alexandersson, M., Hansson, G. C. & Samuelsson, T. Bioinformatic
729 identification of polymerizing and transmembrane mucins in the puffer fish *Fugu rubripes*.
730 *Glycobiology* **14**, 521–527 (2004).
731 19. Johansson, M. E. V. *et al.* Normalization of host intestinal mucus layers requires long-
732 term microbial colonization. *Cell Host Microbe* **18**, 582–592 (2015).
733 20. Engevik, M. A. *et al.* Mucin-degrading microbes release monosaccharides that
734 chemoattract *Clostridioides difficile* and facilitate colonization of the human intestinal
735 mucus layer. *ACS Infect Dis* **7**, 1126–1142 (2021).
736 21. Cantarel, B. I. *et al.* The Carbohydrate-Active EnZymes database (CAZy): An expert
737 resource for glycogenomics. *Nucleic Acids Res* **37**, D233 (2009).

22. Wagner, C. E. *et al.* Comparison of physicochemical properties of native mucus and reconstituted mucin gels. *Biomacromolecules* **24**, 628–639 (2023).
23. Sardelli, L. *et al.* Towards bioinspired *in vitro* models of intestinal mucus. *RSC Adv* **9**, 15887-15899 (2019).
24. Kitamura, H. *et al.* Alteration in mucin gene expression and biological properties of HT29 colon cancer cell subpopulations. *European Journal of Cancer* 32A, 1788-1796 (1996).
25. Lesuffleur, T. *et al.* Differential expression of the human mucin genes MUC1 to MUC5 in relation to growth and differentiation of different mucus-secreting HT-29 cell subpopulations. *J Cell Sci* **106**, 771–783 (1993).
26. Kim, R. *et al.* An in vitro intestinal platform with a self-sustaining oxygen gradient to study the human gut/microbiome interface. *Biofabrication* **12**, 015006 (2020).
27. Wang, Y., Kim, R., Sims, C. & Allbritton, N. Building a thick mucus hydrogel layer to improve the physiological relevance of *in vitro* primary colonic epithelial models. *Cell Mol Gastroenterol Hepatol* **8**, 653-655.e5 (2019).
28. Howard, R. L. *et al.* Biochemical and rheological analysis of human colonic culture mucus reveals similarity to gut mucus. *Biophys J* **120**, 5384–5394 (2021).
29. Cartman, S. T. & Minton, N. P. A mariner-based transposon system for *in vivo* random mutagenesis of *Clostridium difficile*. *Appl Environ Microbiol* **76**, 1103–1109 (2010).
30. Pruss, K. M. & Sonnenburg, J. L. *C. difficile* exploits a host metabolite produced during toxin-mediated disease. *Nature* **593**, 261–265 (2021).
31. Battaglioli, E. J. *et al. Clostridioides Difficile* uses amino acids associated with gut microbial dysbiosis in a subset of patients with diarrhea. *Sci. Transl. Med* **10**, eaam7019 (2018).
32. Aguirre, A. M. & Sorg, J. A. Gut associated metabolites and their roles in *Clostridioides difficile* pathogenesis. *Gut Microbes* **14**, e2094672 (2022).
33. Bouillaut, L., Self, W. T. & Sonenshein, A. L. Proline-dependent regulation of *Clostridium difficile* Stickland metabolism. *J Bacteriol* **195**, 844–854 (2013).
34. Neumann-Schaal, M., Jahn, D. & Schmidt-Hohagen, K. Metabolism the difficile way: The key to the success of the pathogen *Clostridioides difficile*. *Front Microbiol* 10, 219 (2019).
35. Köpke, M., Straub, M. & Dürre, P. *Clostridium difficile* is an autotrophic bacterial pathogen. *PLoS One* **8**, (2013).
36. Gencic, S. & Grahame, D. A. Diverse energy-conserving pathways in *Clostridium difficile*: Growth in the absence of amino acid Stickland acceptors and the role of the Wood-Ljungdahl pathway. *J Bacteriol* **202**, e00233-20 (2020).
37. de Vladar, H. P. Amino acid fermentation at the origin of the genetic code. *Biol Direct* **7**, 6 (2012).
38. Song, Y. *et al.* Functional cooperation of the glycine synthase-reductase and Wood-Ljungdahl pathways for autotrophic growth of *Clostridium drakei*. *Proc Natl Acad Sci USA* **117**, 7516–7523 (2020).
39. Kikuchi, G., Motokawa, Y., Yoshida Ã3, T. & Hiraga, K. Glycine cleavage system: reaction mechanism, physiological significance, and hyperglycinemia. *Proc Jpn Acad* **84**, 7 (2008)
40. Stauffer, G. V. Regulation of serine, glycine, and one-carbon biosynthesis. *EcoSal Plus* **1**, (2004).
41. Ramos, J. L. *et al.* The TetR family of transcriptional repressors. *Microbiology and Molecular Biology Reviews* **69**, 326–356 (2005).
42. Serizawa, M. *et al.* Functional analysis of the YvrGHb two-component system of *Bacillus subtilis*: Identification of the regulated genes by DNA microarray and northern blot analyses. *Biosci Biotechnol Biochem* **69**, 2155-2169 (2005).
43. Pannullo, A. G., Guan, Z., Goldfine, H. & Ellermeier, C. D. HexSDF Is required for synthesis of a novel glycolipid that mediates daptomycin and bacitracin resistance in *C. difficile*. *mBio* **14**, 2 (2023).

44. Fang, C., Stiegeler, E., Cook, G. M., Mascher, T. & Gebhard, S. *Bacillus subtilis* as a platform for molecular characterisation of regulatory mechanisms of *Enterococcus faecalis* resistance against cell wall antibiotics. *PLoS One* **9**, (2014).
45. Kelley, L. A., Mezulis, S., Yates, C. M., Wass, M. N. & Sternberg, M. J. E. The Phyre2 web portal for protein modeling, prediction and analysis. *Nat Protoc* **10**, 845–858 (2015).
46. Esther Jr, C. R. *et al.* Mucus accumulation in the lungs precedes structural changes and infection in children with cystic fibrosis. *Sci Transl Med* **11**, eaav3488 (2019).
47. Markovetz, M. R. *et al.* Mucus and mucus flake composition and abundance reflect inflammatory and infection status in cystic fibrosis. *Journal of Cystic Fibrosis* **21**, 959–966 (2022).
48. Rouillard, K. R. *et al.* Altering the viscoelastic properties of mucus-grown *Pseudomonas aeruginosa* biofilms affects antibiotic susceptibility. *Biofilm* **5**, (2023).
49. Powers, D. A., Jenior, M. L., Kolling, G. L. & Papin, J. A. Network analysis of toxin production in Clostridioides difficile identifies key metabolic dependencies. *PLoS Comput Biol* **19**, (2023).
50. Jenior, M. L. *et al.* Novel Drivers of Virulence in Clostridioides difficile Identified via Context-Specific Metabolic Network Analysis. *mSystems* **6**, (2021).
51. Jenior, M. L., Moutinho, T. J., Dougherty, B. V. & Papin, J. A. Transcriptome-guided parsimonious flux analysis improves predictions with metabolic networks in complex environments. *PLoS Comput Biol* **16**, (2020).
52. Tremblay, Y. D. N. *et al.* Metabolic adaption to extracellular pyruvate triggers biofilm formation in Clostridioides difficile. *ISME Journal* **15**, 3623–3635 (2021).
53. Dubois, T. *et al.* A microbiota-generated bile salt induces biofilm formation in Clostridium difficile. *NPJ Biofilms Microbiomes* **5**, 100104 (2019).
54. Marshall, A., McGrath, J. W., Graham, R. & McMullan, G. Food for thought-The link between *Clostridioides difficile* metabolism and pathogenesis. *PLoS Pathogens* **19**, e1011034 (2023).
55. Antunes, A. *et al.* Global transcriptional control by glucose and carbon regulator CcpA in *Clostridium difficile*. *Nucleic Acids Research* **40**, 10701–10718 (2012).
56. Janoir, C. *et al.* Adaptive strategies and pathogenesis of *Clostridium difficile* from *in vivo* transcriptomics. *Infect Immun* **81**, 3757–3769 (2013).
57. Poquet, I. *et al. Clostridium difficile* biofilm: Remodeling metabolism and cell surface to build a sparse and heterogeneously aggregated architecture. *Front Microbiol* **9**, (2018).
58. Kim, J. & Kim, B. S. Bacterial sialic acid catabolism at the host–microbe interface. *Journal of Microbiology* **61**, 369–377 (2023).
59. Willing, S. E. *et al. Clostridium difficile* surface proteins are anchored to the cell wall using CWB2 motifs that recognise the anionic polymer PSII. *Mol Microbiol* **96**, 596–608 (2015).
60. Anwar, F. & Vedantam, G. Surface-displayed glycopolymers of *Clostridioides difficile*. *Current Opinion in Microbiology* **66**, 86–91 (2022).
61. Percy, M. G. & Gründling, A. Lipoteichoic acid synthesis and function in Gram-positive bacteria. *Annual Review of Microbiology* **68**, 81–100 (2014).
62. Fabretti, F. *et al.* Alanine esters of enterococcal lipoteichoic acid play a role in biofilm formation and resistance to antimicrobial peptides. *Infect Immun* **74**, 4164–4171 (2006).
63. Morrison, Z. A. & Nitz, M. Synthesis of C6-substituted UDP-GlcNAc derivatives. *Carbohydr Res* **495**, 108071 (2020).
64. Gu, Y. *et al.* Rewiring the glucose transportation and central metabolic pathways for overproduction of N-Acetylglucosamine in *Bacillus subtilis*. *Biotechnol J* **12**, 170020 (2017).
65. Brauer, M. *et al.* What's a Biofilm?—How the choice of the biofilm model impacts the protein inventory of *Clostridioides difficile*. *Front Microbiol* **12**, 682111 (2021).

66. Sicard, J. F., Bihan, G. Le, Vogeleer, P., Jacques, M. & Harel, J. Interactions of intestinal bacteria with components of the intestinal mucus. *Front Cell Infect Microbiol* **7**, 387 (2017).
67. Derrien, M., Vaughan, E. E., Plugge, C. M. & de Vos, W. M. *Akkermansia municiphila* gen. nov., sp. nov., a human intestinal mucin-degrading bacterium. *Int J Syst Evol Microbiol* **54**, 1469–1476 (2004).
68. Breton, C., Šnajdrová, L., Jeanneau, C., Koča, J. & Imberty, A. Structures and mechanisms of glycosyltransferases. *Glycobiology* **16**, 29R-37R (2006).
69. Ioannou, A., Knol, J. & Belzer, C. Microbial glycoside hydrolases in the first year of life: An analysis review on their presence and importance in infant gut. *Front Microbiol* **12**, 631282 (2021).
70. Cattoir, V. *et al.* Transcriptional response of mucoid *Pseudomonas aeruginosa* to human respiratory mucus. *mBio* **3**, e00410-12 (2012).
71. Wagner, C. E., Wheeler, K. M. & Ribbeck, K. Mucins and their role in shaping the functions of mucus barriers. *Annu. Rev. Cell Dev. Biol* **34**, 189–215 (2018).
72. Chu, D. & Barnes, D. J. The lag-phase during diauxic growth is a trade-off between fast adaptation and high growth rate. *Sci Rep* **6**, 25191 (2016).
73. Piepenbreier, H., Fritz, G. & Gebhard, S. Transporters as information processors in bacterial signalling pathways. *Molecular Microbiology* **104**, 1–15 (2017).
74. Tremblay, Y. D. & Dupuy, B. The blueprint for building a biofilm the *Clostridioides difficile* way. *Current Opinion in Microbiology* **66**, 39–45 (2022).
75. Semenyuk, E. G. *et al.* Spore formation and toxin production in *Clostridium difficile* biofilms. *PLoS One* **9**, e87757 (2014).
76. Sorg, J. A. & Dineen, S. S. Laboratory maintenance of *Clostridium difficile*. *Curr Protoc Microbiol* **12**, 9A.1.1-9A.1.10 (2009).
77. Girinathan, B. P. *et al.* In vivo commensal control of *Clostridioides difficile* virulence. *Cell Host Microbe* **29**, 1693-1708.e7 (2021).
78. Ruiz, L. M. R. *et al.* Coordinated modulation of multiple processes through phase variation of a c-di- GMP phosphodiesterase in *Clostridioides difficile*. *PLoS Pathog* **18**, e1010677 (2022).
79. Wang, Y. *et al.* Self-renewing monolayer of primary colonic or rectal epithelial cells. *Cell Mol Gastroenterol Hepatol* **4**, 165-182.e7 (2017).
80. Bouillaut, L., McBride, S. M. & Sorg, J. A. Genetic manipulation of *Clostridium difficile*. *Curr Protoc Microbiol* (2011) doi:10.1002/9780471729259.mc09a02s20.
81. Bolger, A. M., Lohse, M. & Usadel, B. Trimmomatic: a flexible trimmer for Illumina sequence data. *Bioinformatics* **30**, 2114–2120 (2014).
82. Wingett, S. W. & Andrews, S. Fastq screen: A tool for multi-genome mapping and quality control . *F1000Res* **7**, 1338 (2018).
83. Langmead, B. & Salzberg, S. L. Fast gapped-read alignment with Bowtie 2. *Nat Methods* **9**, 357–359 (2012).
84. Chung, M. *et al.* FADU: a Quantification Tool for Prokaryotic Transcriptomic Analyses. *mSystems* **6**, 1–16 (2021).
85. Love, M. I., Huber, W. & Anders, S. Moderated estimation of fold change and dispersion for RNA-seq data with DESeq2. *Genome Biol* **15**, 550 (2014).
86. Subramanian, A. *et al.* Gene Set Enrichment Analysis: A knowledge-based approach for interpreting genome-wide expression profiles. *Proc Nat Sci USA* **102**, 15545-15550 (2005).
87. Mootha, V. K. *et al.* PGC-1α-responsive genes involved in oxidative phosphorylation are coordinately downregulated in human diabetes. *Nature Genetics* **34**, 267-273 (2003).

888 88. Garrett, E. M. *et al.* Phase variation of a signal transduction system controls
889 *Clostridioides difficile* colony morphology, motility, and virulence. *PLoS Biol* **17**, 1–28
890 (2019).
891 89. Trzilova, D., Anjuwon-Foster, B. R., Torres Rivera, D. & Tamayo, R. Rho factor mediates
892 flagellum and toxin phase variation and impacts virulence in *Clostridioides difficile*. *PLoS*
893 *Pathog* **16**, 1–28 (2020).
894 90. Mason, T. G. Estimating the viscoelastic moduli of complex fluids using the generalized
895 Stokes-Einstein equation. *Rheol Acta* **39**, 371-378 (2000).
896 91. Hill, D. B. *et al.* A biophysical basis for mucus solids concentration as a candidate
897 biomarker for airways disease. *PLoS One* **9**, e87681 (2014).
898 92. Vyas, H. K. N., McArthur, J. D. & Sanderson-Smith, M. L. An optimised GAS-pharyngeal
899 cell biofilm model. *Sci Rep* **11**, 8200 (2021).
900 93. Purcell, E. B. *et al.* A nutrient-regulated cyclic diguanylate phosphodiesterase controls
901 *Clostridium difficile* biofilm and toxin production during stationary phase. *Infect Immun* **85**,
902 e00347-17 (2017).
903 94. O'Toole, G. A. *et al.* Genetic approaches to study of biofilms. *Can. J. Microbiol* **310**, 91-
904 109 (1999).
905

Supplementary Table 1: Differentially expressed genes related to nutrient acquisition or metabolism. L2FC±SE: Log_2 fold change ± standard error.

Fructose and Mannose Metabolism Gene Set (KEGG)			
Gene	**Name, Description, & Details**	**L2FC±SE**	**p-adj**
CDR0692	*gutA*; Glucitol/sorbitol PTS system EIIC component; homologous to CD630 *srlA*	1.367±0.104	0.0000
CDR0693	*srlE*; Glucitol/sorbitol PTS system EIIB component; homologous to CD630 *srlEa*	1.498±0.116	0.0000
CDR0694	*srlE'*; Glucitol/sorbitol PTS system EIIB component; homologous to CD630 *srlEb*	1.493±0.094	0.0000
CDR0695	*srlB*; Glucitol/sorbitol PTS system EIIA component	1.493±0.114	0.0000
CDR0696	*gutD*; Sorbitol-6-phosphate 2-dehydrogenase; homologous to CD630 *srlD*	1.176±0.162	0.0000
CDR2904	Mannose PTS system EIIC component	1.285±0.067	0.0000
CDR2175	L-fuculose-phosphate aldolase	1.219±0.190	0.0000
CDR2898	*xylA*; Xylose isomerase	1.040±0.082	0.0000
CDR2452	Fructose PTS system EIIA component	-1.073±0.134	0.0000
CDR2976	Fructose PTS system EIIA component	-1.221±0.229	0.0000
Wood-Ljungdahl Pathway			
Gene	**Name, Description, & Details**	**L2FC±SE**	**p-adj**
CDR3174	*hydN1*; electron transport protein	0.441±0.070	0.0000
CDR3175	*hydA*; hydrogenase	0.215±0.066	0.0018
CDR3176	*hydN2*; electron transport protein	0.361±0.075	0.0000
CDR3177	hypothetical protein; homologous to CD630 *fdh*	0.489±0.171	0.0042
CDR3178	*fdhD*; formate dehydrogenase accessory protein	0.214±0.081	0.0115
CDR3179	*fdhF*; formate dehydrogenase	0.503±0.067	0.0000
CDR0648	conserved hypothetical protein; homologous to CD630 *metV*	0.270±0.079	0.0009
CDR0649	putative methylenetetrahydrofolate reductase; homologous to CD630 *metF*	0.270±0.089	0.0034
CDR0643	*cooS*; putative bifunctional carbon monoxide dehydrogenase/acetyl-CoA synthase; homologous to CD630 *acsA*	0.522±0.074	0.0000
CDR0652	putative carbon monoxide dehydrogenase/acetyl-CoA synthase complex, small subunit, homologous to CD630 *acsE*	0.516±0.100	0.0000
CDR0653	putative carbon monoxide dehydrogenase/acetyl-CoA synthase complex, alpha subunit, homologous to CD630 *acsC*	0.853±0.068	0.0000
CDR0654	putative carbon monoxide dehydrogenase/acetyl-CoA synthase complex, methyltransferase subunit, homologous to CD630 *acsE*	0.575±0.064	0.0000
CDR0655	putative carbon monoxide dehydrogenase/acetyl-CoA synthase complex, beta subunit, homologous to CD630 *acsB*	0.460±0.069	0.0000
CDR0111	*ptb;* phosphate butyryltransferase	-0.908±0.078	0.0000
CDR2571	putative propanediol utilization protein; homologous to CD630 *pta*	-0.233±0.069	0.0010
CDR1012	*ackA; acetate kinase*	-0.909±0.058	0.0000
CDR0112	*buk*; butyrate kinase	-0.596±0.064	0.0000
CDR0915	*thlA1*; acetyl-CoA acetyltransferase, homologous to CD630 *thlA*	-0.534±0.077	0.0000
CDR0914	*hbd*; 3-hydroxybutyryl-CoA dehydrogenase	-0.449±0.088	0.0000
CDR0913	*crt2*; 3-hydroxybutyryl-CoA dehydratase	-0.516±0.105	0.0000
CDR0912	*etfA2*; electron transfer flavoprotein alpha-subunit	-0.505±0.079	0.0000
CDR0911	*etfB2*; electron transfer flavoprotein beta-subunit	-0.386±0.083	0.0000
CDR0910	*bcd2*; butyryl-CoA dehydrogenase	-0.248±0.067	0.0003
CDR2800	*adhE*; aldehyde-alcohol dehydrogenase	-0.312±0.060	0.0000
Glycine Cleavage System			

Gene	Name, Description, & Details	L2FC±SE	p-adj
CDR0656	*gcvH*; putative glycine cleavage system H protein	0.458±0.086	0.0000
CDR0650	putative carbon monoxide dehydrogenase/acetyl-CoA synthase complex, dihydrolipoyl dehydrogenase subunit; homologous to CD630 *gcvL*	0.347±0.077	0.0000
CDR1556	*gcvPB*; glycine cleavage system P protein	-0.909±0.077	0.0000
CDR1555	putative bi-functional glycine dehydrogenase/aminomethyl transferase protein, homologous to CD630 *gcvT*	-0.601±0.068	0.0000
CDR2615	*glyA*; putative serine hydroxymethyltransferase	0.366±0.070	0.0000
CDR3082	*sdaB*; L-serine dehydratase	0.707±0.067	0.0000
Proline and Glycine Reductases (Stickland Metabolism)			
Gene	**Name, Description, & Details**	**L2FC±SE**	**p-adj**
CDR3097	*prdF*; putative proline racemase	-1.793±0.061	0.0000
CDR3098	conserved hypothetical protein	-2.229±0.064	0.0000
CDR3099	conserved hypothetical protein	-2.180±0.089	0.0000
CDR3100	conserved hypothetical protein	-2.204±0.069	0.0000
CDR3101	*prdB*; proline reductase	-2.245±0.061	0.0000
CDR3103	*prdA*; proline reductase subunit protein	-2.224±0.070	0.0000
CDR3104	*prdR*; sigma-54-dependent transcriptional activator	-0.691±0.083	0.0000
CDR3105	*prdC*; putative electron transfer protein	-1.249±0.083	0.0000
CDR2234	LysR-family regulatory protein	0.556±0.103	0.0000
CDR2235	putative membrane protein	0.421±0.143	0.0036
CDR2236	putative Xaa-Pro dipeptidase	0.258±0.085	0.0034
CDR2237	*grdD*; glycine/sarcosine/betaine reductase complex component C alpha subunit	-3.460±0.070	0.0000
CDR2238	*grdC*; glycine/sarcosine/betaine reductase complex component C beta subunit	-3.306±0.081	0.0000
CDR2239	*grdB*; glycine reductase complex component B gamma subunit	-1.207±0.078	0.0000
CDR2240	*grdA*; glycine/sarcosine/betaine reductase complex component A	-2.292±0.073	0.0000
CDR2241	*grdE*; glycine reductase complex component B alpha and beta subunits	-3.399±0.073	0.0000
CDR2242	*trxA2*; thioredoxin	-3.148±0.101	0.0000
CDR2243	*trxB3*; thioredoxin reductase	-3.155±0.071	0.0000
CDR2244	*grdX*; putative glycine reductase complex component	-2.502±0.085	0.0000

Supplementary Table 2: Differentially expressed genes related to transcriptional regulation or sensing. L2FC±SE: Log_2 fold change ± standard error.

Transcriptional Regulators			
Gene	**Name, Description, & Details**	**L2FC±SE**	**p-adj**
CDR0508	TetR-family transcriptional regulator	2.010±0.072	0.0000
CDR1650	putative transcriptional regulator	1.670±0.072	0.0000
CDR1351	putative transcriptional regulator	1.610±0.167	0.0000
CDR1936	GntR-family transcriptional regulator	1.574±0.098	0.0000
CDR1579	TetR-family transcriptional regulator	1.541±0.071	0.0000
CDR0865	GntR-family transcriptional regulator	1.534±0.104	0.0000
CDR1467	MarR-family transcriptional regulator	1.410±0.077	0.0000
CDR0310	TetR putative transcriptional regulator	1.367±0.089	0.0000
CDR1646	TetR-family transcriptional regulator	1.273±0.076	0.0000
CDR2050	putative transcriptional regulator	1.216±0.140	0.0000
CDR0317	ArsR-family transcriptional regulator	1.194±0.087	0.0000
CDR2553	AraC-family transcriptional regulator	1.185±0.085	0.0000
CDR1619	putative transcriptional regulator	1.171±0.117	0.0000
CDR2450	MerR-family transcriptional regulator	1.147±0.076	0.0000
CDR1950	putative transcriptional regulator	1.121±0.142	0.0000
CDR3274	GntR-family transcriptional regulator	1.106±0.108	0.0000
CDR0991	PadR-family transcriptional regulator	1.105±0.216	0.0000
CDR3067	MarR-family transcriptional regulator	1.083±0.095	0.0000
CDR1259	sigma-54 dependent regulatory protein	1.044±0.092	0.0000
CDR1504	GntR-family transcriptional regulator	1.026±0.267	0.0001
CDR2599	LysR-family transcriptional regulator	1.011±0.090	0.0000
CDR0506	TetR-family transcriptional regulator	-1.021±0.085	0.0000
CDR3197	GntR-family transcriptional regulator	-1.041±0.117	0.0000
CDR0745	GntR-family transcriptional regulator	-1.074±0.088	0.0000
CDR0817	GntR-family transcriptional regulator	-1.091±0.076	0.0000
CDR0373	sigma-54-dependent transcriptional regulator	-1.173±0.083	0.0000
CDR1311	GntR-family transcriptional regulator	-1.197±0.118	0.0000
CDR2781	GntR-family transcriptional regulator	-1.313±0.092	0.0000
CDR2975	AraC-family transcriptional regulator	-1.343±0.179	0.0000
CDR2929	*treR*; GntR-family transcriptional regulator	-1.635±0.142	0.0000
CDR2847	putative transcriptional regulator	-1.740±0.119	0.0000
Sigma Factors			
Gene	**Name, Description, & Details**	**L2FC±SE**	**p-adj**
CDR1348	*rpoD2*; RNA polymerase sigma factor RpoD	1.259±0.136	0.0000
CDR0050	*sigH*;RNA polymerase sigma-H factor	-1.259±0.066	0.0000
Transcription Antierminators			
Gene	**Name, Description, & Details**	**L2FC±SE**	**p-adj**
CDR2970	*bglG2*; transcription antiterminator	1.469±0.149	0.0000
CDR0690	putative transcription antiterminator	1.128±0.143	0.0000
CDR2222	*mtlR;* putative transcription antiterminator	1.036±0.087	0.0000
CDR0054	*nusG*; transcription antitermination protein	-1.098±0.075	0.0000
CDR2977	transcription antiterminator	-1.241±0.155	0.0000
Two Component Systems			
Gene	**Name, Description, & Details**	**L2FC±SE**	**p-adj**
CDR1476	putative two-component histidine kinase	1.557±0.098	0.0000
CDR1569	two-component sensor histidine kinase	1.260±0.141	0.0000
CDR1568	two-component response regulator	1.198±0.140	0.0000
CDR2187	two-component sensor histidine kinase	-1.393±0.079	0.0000
CDR0869	two-component system response regulator	-1.447±0.132	0.0000

CDR2188	two-component system response regulator	-1.679±0.108	0.0000
CDR2020	two-component sensor histidine kinase	-2.049±0.072	0.0000
CDR2021	two-component system response regulator	-2.372±0.089	0.0000
CDR2610	*hexK*; two-component sensor histidine kinase	-3.268±0.092	0.0000
CDR2611	*hexR;* two-component response regulator	-3.286±0.094	0.0000
CDR2206	two-component sensor histidine kinase	-4.054±0.119	0.0000
CDR2205	two-component response regulator	-5.025±0.122	0.0000